



1 **Large ensemble simulations of the North American and Greenland ice**  
2 **sheets at the Last Glacial Maximum with a coupled atmospheric general**  
3 **circulation-ice sheet model**

4

5 Sam Sherriff-Tadano<sup>1</sup>, Ruza Ivanovic<sup>1</sup>, Lauren Gregoire<sup>1</sup>, Charlotte Lang<sup>2</sup>, Niall Gandy<sup>1,5</sup>, Jonathan  
6 Gregory<sup>2,3</sup>, Tamsin L. Edwards<sup>4</sup>, Oliver Pollard<sup>1</sup> and Robin S. Smith<sup>2</sup>

7 <sup>1</sup> School of Earth and Environment, University of Leeds, UK

8 <sup>2</sup> National Centre for Atmospheric Science, University of Reading, UK

9 <sup>3</sup> Met Office Hadley Centre, Exeter, UK

10 <sup>4</sup> King's College London, UK

11 <sup>5</sup> Department of Natural and Built Environment, Sheffield Hallam University, UK

12

13 *Correspondence to:* Sam Sherriff-Tadano (tadanosam@gmail.com)

14

15 **Abstract**

16 The Last Glacial Maximum (LGM) is characterised by huge ice sheets covering the Northern Hemisphere, especially over  
17 North America, and by its cold climate. Numerical simulations of the climate and ice sheets of the LGM have been  
18 performed to better understand these systems, however the inherent uncertainty and sensitivity in the simulations to the  
19 selection of model parameters remain uncertain. Here, we perform a 200-member ensemble of simulations of the North  
20 American and Greenland ice sheets and climate of the LGM with an ice sheet-atmosphere-slab ocean coupled model  
21 (FAMOUS-BISICLES) to explore sensitivities of the coupled climate-ice system to 16 uncertain parameters. In the ensemble  
22 of simulations, the global temperature is primarily controlled by the combination of parameters in the large-scale  
23 condensation scheme and the cumulus convection scheme. In simulations with plausible LGM global temperatures, we find  
24 that the albedo parameters have only a small impact on the Greenland ice volume due to the limited area of surface ablation  
25 associated with the cold climate. Instead, the basal sliding law controls the ice volume by affecting ice transport from the  
26 interior to the margin. On the other hand, like the Greenland ice sheet in future climate change, the LGM North American ice  
27 sheet volume is controlled by parameters in the snow and ice albedo scheme. Few of our simulations produce an extensive  
28 North American ice sheet when the global temperature is above 12°C. Based on constraints on the LGM global temperature,  
29 the ice volume and the southern extent of the North American ice sheet, we select 16 acceptable simulations. These  
30 simulations lack the southern extent of ice compared to reconstructions, though show reasonable performance on the ice  
31 sheet configuration and ice streams facing the Baffin Bay and the Arctic Ocean. The strong sensitivities of the North  
32 American ice sheet to albedo at the LGM may imply a potential constraint on the future Greenland ice sheet by constraining  
33 the albedo schemes.

34



35 **1. Introduction**

36 The rise in sea level predicted in the next several centuries associated with increasing greenhouse gases and global warming  
37 is one of the largest concerns of society and the climate community. The most recent IPCC WG1 report projects a global  
38 mean sea-level rise of more than 3 m under the high end of the increase in radiative forcing (SSP5-8.5) in the next 300 years  
39 (IPCC 2021). However, there are still large uncertainties in the predicted sea level rise with the possibility of a much larger  
40 magnitude (Edwards et al. 2021). This large uncertainty in the projection of sea-level rise reflects the present limited state of  
41 knowledge of several important processes, such as nonlinear behaviours in the ice sheet system (Gregoire et al. 2012, Abe-  
42 Ouchi et al. 2013, Golledge et al. 2019) and interactions of the climate and the ice sheets, which are expressed in climate-ice  
43 sheet coupled models (Deconto and Pollard 2016, Golledge et al. 2019, Gregory et al. 2020, Smith et al. 2021). This  
44 uncertainty shows the importance of improving our understanding of the ice sheet-climate coupled system and to refine  
45 numerical models used for the future projection of climate and sea-level rise.

46  
47 One method of evaluating climate-ice sheet coupled models and improving understanding of the climate-ice sheet coupled  
48 system is to simulate conditions of past periods. In this regard, the Last Glacial Maximum (LGM), which corresponds to  
49 approximately 21 thousand years before present (ka BP; Clark et al. 2009, Kageyama et al. 2021), is useful since both  
50 climate conditions and the ice sheet configurations are relatively well documented compared to previous periods of  
51 glaciation (Tarasov et al. 2012, Kageyama et al. 2021). It has been suggested that the LGM could be used to constrain the  
52 climate sensitivity (Tierney et al. 2020), cloud processes (Zhu et al. 2022) and deep ocean circulation (Sherriff-Tadano et al.  
53 2023), implying that understanding this period has the potential to help constrain climate and ice sheet models and future  
54 sea level projections. During this period, weaker summer insolation and lower concentrations of greenhouse gases caused the  
55 climate to be colder, allowing ice sheets to expand over North America and Northern Europe. As a result, the global climate  
56 was colder by 1.7°C to 8.3°C (Holden et al. 2010, Schmittner et al. 2011, Tierney et al. 2020, Paul et al. 2021) and global  
57 mean sea level was approximately 120 m lower compared to modern (Clark et al. 2009, Gowan et al. 2021). The mass of the  
58 Greenland ice sheet is thought to have been larger by approximately by 2 to 5 m sea level equivalent (SLE) at the LGM  
59 (Clark and Mix 2002, Lecavalier et al. 2014, Bradley et al. 2018, Tabone et al. 2018) and of the Antarctic ice sheet by 5.6 to  
60 14.3 m SLE (e.g. Briggs et al. 2014). The Eurasian ice sheet is thought to have attained a volume of 24 m SLE (Hughes et al.  
61 2016), but by much the largest part of the 120 m SLE is attributed to the growth of the North American ice sheet (at least 60  
62 m SLE, e.g. Abe-Ouchi et al. 2015). The position of the margin of the North American ice sheet is constrained reasonably  
63 well by geological evidence and this line of evidence is often used to validate the performance of ice sheet models (e.g.,  
64 Dyke et al. 2002, Clark et al. 2009).

65  
66 Studies that simulate LGM climate and ice-sheets have primarily treated these components independently using individual  
67 numerical models. To investigate the effect of ice sheets on climate, following Manabe and Broccoli (1985), many  
68 simulations have been performed and compared their simulations with climate models as part of the Paleoclimate Model  
69 Intercomparison Project (PMIP, Braconnot et al. 2007, 2012, Ivanovic et al. 2016, Kageyama et al. 2017). In these  
70 simulations, the ice sheet configuration was specified as a boundary condition and they show the important role of the  
71 existence of the glacial ice sheets on the climate, affecting surface temperature, precipitation, atmospheric and oceanic  
72 circulation (Klockmann et al. 2016, Gregoire et al. 2018, Ivanovic et al. 2018, Sherriff-Tadano et al. 2021). To investigate  
73 the effect of climate on ice sheets, simulations of the LGM ice sheets have been performed with ice sheet models. These  
74 simulations were performed either as full glacial cycle experiments (e.g. Abe-Ouchi et al. 2007) or perpetual LGM  
75 experiments (e.g. Alder and Hostetler 2019). In these experiments, the ice sheet models were forced with climatic conditions  
76 based on outputs from general circulation models (Gregoire et al. 2012, Abe-Ouchi et al. 2013, Alder and Hostetler 2019,  
77 Niu et al. 2019, Blasco et al. 2021). They showed the critical effects of uncertain climatic conditions and albedo in causing a



78 large diversity in the simulated ice sheet configuration (Abe-Ouchi et al. 2007, Alder and Hostetler 2019, Niu et al. 2019,  
79 Blasco et al. 2021) together with uncertainties in basal sliding law (Gandy et al. 2020). These studies highlighted the strong  
80 interaction of climate and ice sheets and the importance of performing simulations with climate-ice sheet coupled models to  
81 better understand the coupled system.

82

83 Recent efforts in the modelling community in developing coupled climate-ice sheet models (e.g. Gregory et al. 2012, Ziemen  
84 et al. 2014, Roche et al. 2014, Smith et al. 2021) mean that higher complexity coupled climate-ice simulations of the glacial  
85 period than have previously been possible may now be performed. Gregory et al. (2012) performed simulations of an ice  
86 sheet inception over North America with the climate-ice sheet coupled model FAMOUS-Glimmer. They showed the role of  
87 the albedo on the magnitude and speed of the inception. Ziemen et al. (2014) performed simulations of the ice sheet-  
88 atmosphere-ocean with a more complex ice sheet-climate coupled model. Their simulation reproduced the climate and the  
89 ice sheets of the LGM reasonably well, while the southern extent of the North American ice sheet was somewhat smaller  
90 compared to reconstructions. This is partly due to the relatively coarse resolution of the atmospheric model (Ziemen et al.  
91 2014), which means their model underestimated the stationary wave effect that cools the southern extent of the North  
92 American ice sheet and hence underestimates the ice area in that region (Roe and Lindzen 2001, Abe-Ouchi et al. 2007).  
93 Lofverstrom et al. (2015) performed simulations of the North American ice sheet and climate with an atmosphere-ice sheet-  
94 slab ocean coupled model in an idealised framework and showed the importance of interactions between atmospheric  
95 circulation, the Rocky Mountains and the ice sheet in shaping the ice sheet's zonally asymmetric features. Willeit and  
96 Ganopolski (2016) presented simulations of the last glacial cycle with an ice sheet model coupled to an Earth System model  
97 of intermediate complexity and discussed the role of the darkening effect of snow. Quiquet et al. (2021) performed  
98 simulations of the ice sheets and climate of the LGM and the last deglaciation with a coupled climate-ice sheet model. They  
99 managed to reproduce the overall characteristics of the evolution of climate and ice sheets and showed the effects of  
100 modulations in the oceanic circulation.

101

102 These previous studies provide very useful insight into the physical interactions within the coupled system, but the inherent  
103 uncertainty and sensitivity in the simulations to the selection of model inputs (including physical parameterisations) remain  
104 untested as in all of these studies a single version of a given model was used. Perturbed parameter ensembles of simulations  
105 are a powerful way to estimate uncertainties originating from particular parameter values in a single model (Murphy et al.  
106 2004, Sanderson 2011, Shiogama et al. 2012). For example, Rougier et al. (2009) analysed results from an ensemble  
107 performed under modern and future climate conditions with an atmosphere-slab ocean coupled general circulation model  
108 (HadSM3) and showed the critical role of entrainment rate in the cumulus cloud scheme and its interaction with large-scale  
109 condensation scheme on global climate. Gregoire et al. (2011) performed an ensemble of simulations with an atmosphere-  
110 ocean coupled general circulation model, FAMOUS, and found that the mid-latitude cloud parameters and sea ice albedo  
111 exert an important influence on global cooling at the LGM. Furthermore, they used their results to identify combinations of  
112 parameter values that optimise model skill in simulating both the pre-industrial and LGM, thus improving model flexibility.  
113 Gandy et al. (2023) recently performed ensemble simulations of the North American ice sheet and climate with an  
114 atmosphere-ice sheet coupled model FAMOUS-Ice (Smith et al. 2021). They showed the importance of ice and snow albedo  
115 in building the ice sheet due to strong summer insolation at the southern margin of the North American ice sheet. In this  
116 study, however, the sea surface temperature and the global temperature were fixed. As a result, the role of clouds on the  
117 climate and the effects of global mean temperature on the ice sheet volume remained unclear.

118

119 Here, we perform a large ensemble of simulations of the North American and Greenland ice sheets and climate of the LGM  
120 with a version of the FAMOUS-Ice coupled atmosphere-ice sheet model, which utilises the ice sheet model BISICLES rather



121 than Glimmer (Method, e.g. Smith et al. 2021). With this model, we estimate the impact of uncertainty in the choice of  
122 parameter values implemented in the atmosphere and ice sheet components of the model and test the ability of the model to  
123 simulate ice sheets and climates very different from today. The results are evaluated against the LGM global mean  
124 temperature, ice volume and southern extent of the North American ice sheet. Through these experiments, we aim to address  
125 the following questions;

- 126 • How do uncertain parameters affect the climate and ice sheets at the LGM?
- 127 • Is there a difference in important parameters between the North American and Greenland ice sheets?
- 128 • How well are the ice sheets simulated in this experiment, e.g. in terms of North American ice sheet volume, the  
129 southern extent of the North American ice sheet and the position of the ice streams?

130

131 The remainder of the paper is structured as follows. Section 2 gives a description of the model, the experimental design and  
132 the integration procedure. Section 3 reports on the results of the large ensemble. Section 4 discusses the results and the effect  
133 of biases in the model. Lastly, section 5 gives the conclusions.

134

## 135 2. Method

### 136 2.1 Model

137 Our simulations of the climate and ice sheets are performed with the atmosphere-ice sheet-slab ocean coupled model,  
138 FAMOUS-Ice (Smith et al. 2021, Gregory et al. 2020). FAMOUS is a low-resolution version of the atmosphere-ocean  
139 general circulation model (AOGCM) HadCM3; the horizontal resolution is  $7.5^\circ$  in longitude and  $5^\circ$  in latitude (Smith et al.  
140 2008, 2012). Due to the lower resolution, FAMOUS runs 10 times faster compared to HadCM3, while retaining a reasonable  
141 performance for the modern and the LGM climates (Smith et al. 2008, 2012, Smith and Gregory 2012). Benefitting from  
142 much cheaper computational cost, it is feasible to run multi-millennial simulations (Smith and Gregory 2012) and large  
143 ensembles (Gregoire et al. 2011), as required to meet our objectives.

144

145 The latest version of FAMOUS (FAMOUS-ice, Smith et al. 2021) incorporates a downscaling scheme for the calculation of  
146 the surface mass balance (SMB) over ice sheets. In the downscaling scheme, 10 additional vertical tiles are added to better  
147 represent the elevation dependence of surface temperature and downward longwave radiation, following the method first  
148 used in Vizcaino et al. (2013). The downscaled temperature and longwave radiation are then utilised with downward  
149 shortwave radiation to calculate the SMB based on a surface energy budget scheme, together with precipitation from the  
150 original FAMOUS grid. The model also incorporates an updated snow and ice albedo scheme, which accounts for albedo  
151 changes associated with modifications in surface air temperature (*daice*), grain size (*avgr*) and density of the snow (*fsnow*)  
152 (Smith et al. 2021, Table 1). As a result, the atmospheric model reproduces the general pattern of SMB over the modern  
153 Greenland ice sheet reasonably well (van de Wal et al. 2012, Smith et al. 2021) with some overestimating biases in the  
154 elevation of Equilibrium-Line Altitude (ELA; Smith et al., 2021, see also subsection 4.2).

155

156 Previous work with FAMOUS-ice used prescribed climatological SSTs and sea-ice instead of an interactive ocean model  
157 (Gregory et al., 2020; Smith et al., 2021, Gandy et al. 2023). In the present study, we use a slab ocean model with the same  
158 horizontal resolution as the atmosphere. Inclusion of a slab ocean model allows the local and global SST and sea-ice to vary  
159 in response to changes in climate, which in our experiments are caused by modifications in parameters and the advance and  
160 retreat of ice sheets. In the slab ocean model, sea-ice is advected by the climatological monthly surface sea-water velocity of  
161 the HadCM3 pre-industrial control experiment, with sea-ice convergence prevented when the local thickness exceeds 4.0 m.



162 The local thickness of sea ice evolves due to snowfall, sublimation and melting at the surface, and melting and freezing at  
163 the base in response to heat exchange with the slab ocean. The SST is the temperature of a layer of water 50 m thick, and  
164 evolves in response to surface energy exchange with the atmosphere and heat transport within the slab ocean. Since the slab  
165 ocean does not simulate ocean dynamics, climatological heat transport is prescribed within it as a monthly climatological  
166 field of heat convergence. The heat convergence field is obtained from a calibration experiment (Section 2.2) in which the  
167 model calculates the heat flux necessary to maintain a reference climatological state of SST and sea-ice.

168

169 The slab ocean model is essentially the same as described by Williams et al. (2001), where it is used with the HadCM3  
170 AGCM, but the present study is the first to use it with the atmosphere resolution of FAMOUS. For this configuration, grid  
171 boxes which are partly land and partly sea were implemented in the slab ocean, as in the AGCM. In order to prevent unstable  
172 surface temperature feedbacks in coastal grid boxes with small sea fraction, we found that horizontal diffusion of heat in the  
173 slab ocean was needed (diffusivity  $10000 \text{ m}^2 \text{ s}^{-1}$ ); unlike the prescribed heat convergence, diffusive heat divergence responds  
174 to the time-dependent slab temperature gradient and thus dissipates local anomalies, but usually it is much smaller than the  
175 heat convergence. In order to prevent local build-up of excessively thick coastal sea ice, we allow horizontal diffusion of sea  
176 ice thickness (diffusivity  $5000 \text{ m}^2 \text{ s}^{-1}$ ) when the local thickness exceeds 4.0 m. To improve the reproduction of the reference  
177 sea-ice climatology, we adjusted the coefficients for sea-ice basal melting.

178

179 Instead of Glimmer, we use the more complex and computationally demanding BISICLES ice sheet model (Cornford et al.  
180 2013). BISICLES is a vertically integrated ice sheet model, which has been mainly used for simulations of modern and  
181 future Greenland (Lee et al. 2015, Smith et al. 2021b) and Antarctica (Martin et al. 2019, Smith et al. 2021b), and has  
182 recently been applied for reproducing past ice sheets over North America (Matero et al. 2020) and Northern Europe (Gandy  
183 et al. 2018, 2019, 2020). Whereas Glimmer uses the shallow ice approximation, BISICLES applies a L1L2 approximation,  
184 which allows more flexibility in sliding and flowing of the ice sheet especially at the ice shelf area (Cornford et al. 2013). In  
185 addition, the model is capable of changing spatial resolution according to the flow regime of the ice. In this study, a  
186 horizontal resolution of 32 km is chosen, with refinement to 16 km at ice sheet margins. The choice of the resolution was  
187 made based on practical reasons regarding the computational expense. We show that this resolution is adequate for  
188 simulating large-scale glaciers in the northern area of the North American ice sheet (see subsection 4.1).

189

190 We utilise a basal drag scheme introduced by Gandy et al. (2019), which explicitly expresses the thermodynamic interaction  
191 of the ice sheets and the underlying till. This scheme combines the Coulomb-friction law and Weertman-friction law  
192 depending on the water pressure in the bedrock sediment (Tsai et al. 2015). The basal drag follows the Weertman law under  
193 cold ice basal temperature and dry bedrock sediment. Under warm ice basal temperature and wet bedrock sediment, the basal  
194 drag follows the Coulomb-friction law. Depending on the depth of till water in the sediment, the friction of ice and bedrock  
195 changes. The depth of the till water is controlled by the balance of basal melting of the ice sheet and a parameter (*drain*) that  
196 controls the vertical till-stored drainage rate. Using this basal scheme in BISICLES simulations, Gandy et al. (2019)  
197 reproduced the features of known ice streams in the LGM British ice sheet.

198

199 Changes in ice-sheet geometry, and the subsequent redistribution of the Earth's surface mass load, result in deformation of  
200 the Earth's topography through a series of interconnected processes known as glacial isostatic adjustment (GIA). An  
201 important impact of GIA for the purpose of ice-sheet modelling is the subsidence of the bedrock topography beneath an ice-  
202 sheet. The rate of the solid Earth response towards isostatic equilibrium, which can range from centuries to millions of years,  
203 is viscoelastic in nature as a result of the rheological structure of the Earth and specific pattern of ice loading. In order to  
204 simulate the first-order effects of GIA on bedrock topography, we couple the ice-sheet model to a simple Elastic Lithosphere



205 Relaxing Asthenosphere (ELRA) model which approximates this response by assuming a fully elastic lithosphere above a  
206 uniformly viscous asthenosphere (Kachuck et al. 2020). A relaxation time of 3000 years is applied in this model based on  
207 previous studies (Pollard and Deconto 2012).

208

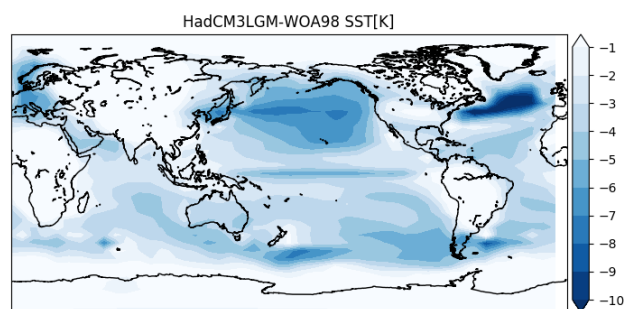
209 In running FAMOUS-BISICLES, a 10 times acceleration is applied to the ice sheet model to save computational cost  
210 (Gregory et al. 2012, Ziemen et al. 2014). In this method, the ice sheet model is integrated for 10 years using 1-year of  
211 climate simulation by FAMOUS. Gregory et al. (2012) and Gregory et al. (2020) show that 10 times acceleration has a small  
212 to negligible impact on the simulated ice sheet evolution, supporting the use of this technique.

## 213 2.2 Experimental design

214 Our experiments mainly follow the protocol of PMIP4 LGM simulations (Kageyama et al. 2017, 2021), which specifies the  
215 insolation, atmospheric concentration of Greenhouse gases ( $\text{CO}_2=190$  ppm,  $\text{CH}_4=375$  ppb,  $\text{NO}_2=200$  ppb, all by volume) and  
216 configurations of continental ice sheets. With respect to ice sheets, in our setup, only the Eurasian and Antarctica ice sheets  
217 are fixed to the reconstruction of GLAC-1D (Tarasove et al. 2012) as the Laurentide and Greenland ice sheets are simulated  
218 with BISICLES. While the protocol specifies the insolation forcing of 21 ka BP, here we use the insolation of 23 ka since the  
219 ice sheet at the LGM is likely still adjusting to earlier forcing (Abe-Ouchi et al. 2013).

220

221 For calibrating the slab heat convergence (Section 2.1), we use the SST and sea-ice climatology from a previous LGM  
222 simulation performed with HadCM3, shown in Fig. 1 (Izumi et al., 2022). The simulated SST field exhibits a cold LGM  
223 climate, having a global cooling of 6.5 K. This value is similar to Tierney et al. (2020), who estimate 6.5 K to 5.7 K. For  
224 simplicity of design and clarity of interpretation, the oceanic heat flux is fixed among all the ensemble simulations, thus  
225 assuming no changes in the oceanic heat transport in response to the different parameter values in each member.



226

227 Fig. 1 Annual mean sea surface temperature anomaly fields (K, colour) between a HadCM3 LGM simulation and modern  
228 observation (World Ocean Atlas 1998). The sea surface temperature field from HadCM3 is used as the target sea surface  
229 condition for our prescribed slab ocean setup.

230

231 We perform 200-member ensemble simulations by varying 16 parameter values associated with climate and ice dynamics, as  
232 summarised in Table 1, using a Latin-hypercube sampling method (Williamson 2015). The choice and the range of the  
233 parameter values in FAMOUS are modified following Gregoire et al. (2012) and Gandy et al. (2023). In BISICLES, the  
234 range of sliding law parameters are modified following sensitivity experiments of Gandy et al. (2019). For *drain*, which  
235 specifies the vertical till-stored drainage rate, the value is very uncertain and hence we varied it to ensure that the till of the  
236 interior of the ice sheet remains dry. Much lower values for *drain*, as used in Gandy et al. (2019) in their simulation of the  
237 much smaller British-Irish ice sheet, result in unphysically wet basal conditions and fast sliding in our simulations so we



238 used a higher range. For  $n$ , which specifies the coefficient in Glen’s flow law, the range is selected in a practical way;  
 239 applying a high value increases the calculation time by more than 10 times due to very large ice velocities and the resulting  
 240 refinement in several locations. Hence, the range of  $n$  is necessarily capped for its upper limit at 3.1, where our technical  
 241 tests indicated that the simulations will most likely complete within a feasible run length (two months of wallclock time).  
 242 During the ice sheet spin-up phase (see subsection 2.3) we specify a constant SMB. The value of this  $smb$  is varied across the  
 243 ensemble so that the ice volume at the initiation of FAMOUS-BISICLES coupling has a spread of 25 m SLE, which is  
 244 similar to the uncertainty in the global ice volume estimates at the LGM (e.g. Abe-Ouchi et al. 2015). Two-hundred sets of  
 245 parameter value combinations for these 16 parameters are sampled using a Latin hypercube sampling method, assuming a  
 246 uniform value probability across each parameter range, to explore across the full ranges of the 16-dimensional parameter  
 247 space.

248

249 For simplicity, we apply a single value, spatially uniform basal heat flux of  $158 \text{ mW/m}^2$  and  $100 \text{ W/m}^2$  under the grounded  
 250 and floating ice respectively. However this needs to be reassessed in the future as both the basal heat flux over the continent  
 251 (e.g. Margold et al. 2018) and the ocean can vary spatially.

252

253 Table 1 Summary of parameters modified in the ensemble simulations. ND stands for non dimensional.

Name	Min value	Max value	Unit	Note
daice	-0.4	0.05	$K^{-1}$	Darkening effect of warm surface air temperature on bare ice in the albedo scheme, mimicking water collecting at the surface. Minimum value reduces the bare ice albedo to as low as 0.15 (Smith et al. 2021).
fsnow	350	799	$kg \text{ m}^{-3}$	Density threshold for snow in the albedo scheme beyond which the surface starts to be regarded as bare ice. Higher values correspond to using brighter albedoes for denser snow and tends to increase ice sheet albedo (Smith et al. 2021).
avgr	0.001	0.01	$\mu\text{m}^{-3}$	Dependence of snow albedo on increasing grain size. Higher value enhances the darkening of snow over time and reduces the snow albedo (Smith et al. 2021).
rhcrit	0.6	0.9	ND	Threshold of relative humidity to form large-scale clouds (Smith, 1990).
Vfl	0.5	2.0	$\text{m s}^{-1}$	Speed of ice sedimentation (Heymsfield, 1977).
ct	0.00005	0.0004	$\text{s}^{-1}$	Conversion rate of cloud liquid water droplets to precipitation (Smith, 1990)
cw	0.0001	0.002	$kg \text{ m}^{-3}$	Threshold value of cloud liquid water for formation of precipitation (Smith, 1990). Only values over land are modified.
entcoef	0.6	6.0	ND	Entrainment rate coefficient. Higher value enhances mixing of an ascending convective plume with ambient dry air.
tgrad	-0.01	-0.002	$K \text{ m}^{-1}$	Air temperature lapse rate used during the downscaling to ice sheet surfaces. Larger negative values correspond to stronger lapse rate effects (Smith et al. 2021).
alpham	0.2	0.65	ND	The lowest value of albedo in the sea ice scheme.
seaiice	0.00015	0.00035	$\text{m}^2 \text{ s}^{-1}$	Efficiency of heat exchange between the base of sea ice and ocean. Higher value increases the heat flux and causes a retreat of sea ice.

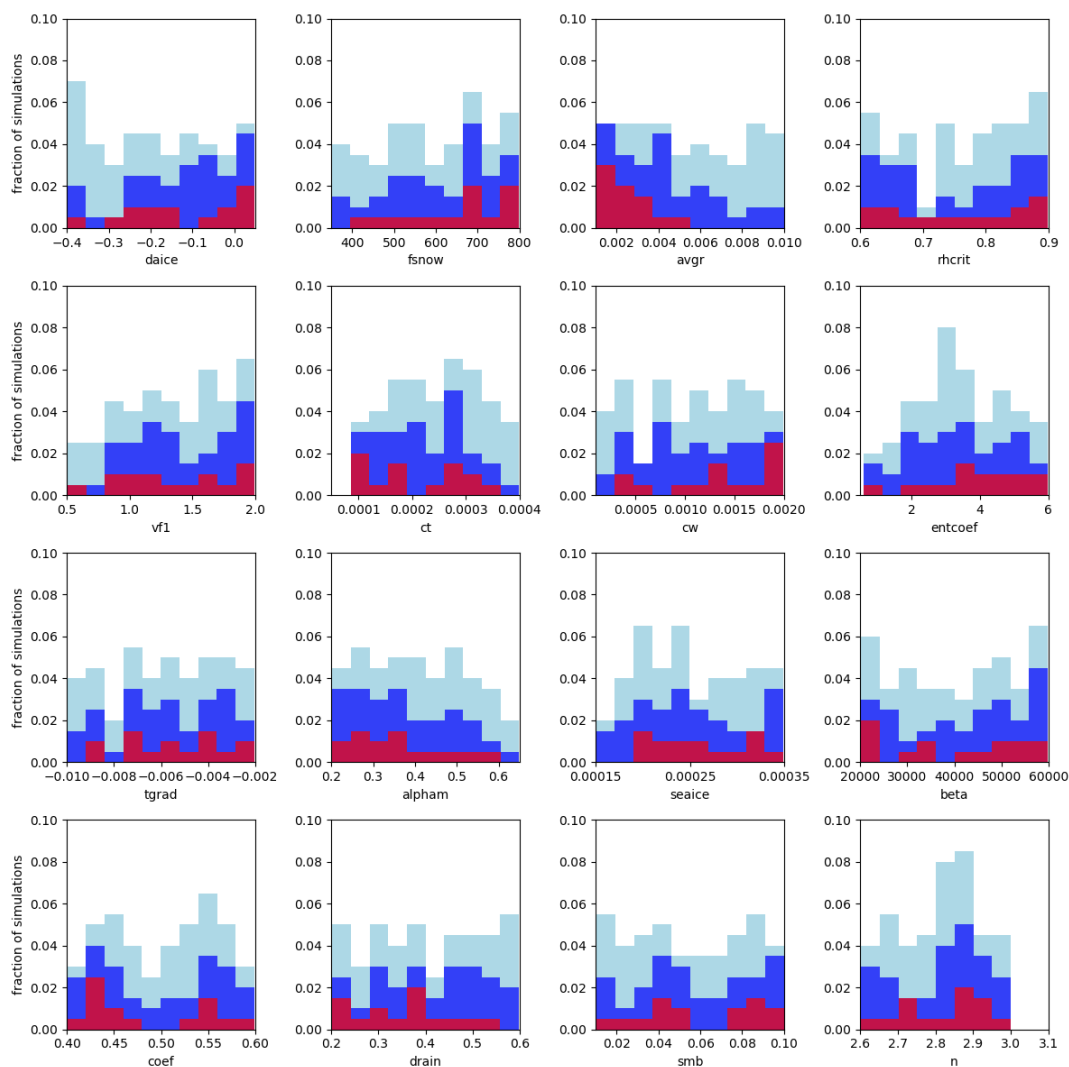




beta	20000	60000	$Pa m^{1/3} a^{1/3}$	Coefficient in Weertman-friction law. Higher value corresponds to stronger friction between the ice base and the dry bedrock (Gandy et al. 2019).
coef	0.4	0.6	<i>ND</i>	Coefficient in Coulomb-friction law (Gandy et al. 2019).
drain	0.2	0.6	$m yr^{-1}$	Magnitude of drainage removing water from the till. Higher value removes water rapidly from the till hence increases the Coulomb-friction (Gandy et al. 2019).
smb	0.01	0.1	$m yr^{-1}$	Magnitude of temporally constant and spatially uniform surface mass balance applied during the standalone BISICLES spin-up. Higher values result in a larger ice sheet at the beginning of the FAMOUS-BISICLES coupled simulation.
n	2.6	3.1	<i>ND</i>	Coefficient in Glen's flow law.

254

255



256

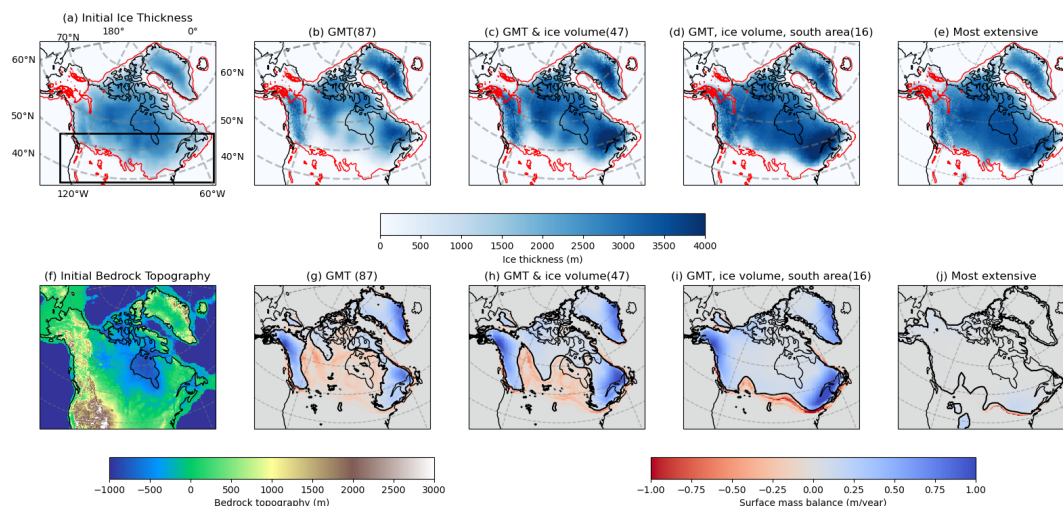




257 Fig. 2 Fraction of the 200 simulations which satisfy the constraints as a function of each of the parameters. 200 members are  
 258 uniformly distributed in each parameter range based on the latin-hypercube sampling method (approximately 20 simulations  
 259 per each parameter bin). Light blue: ensemble members satisfying the global temperature constraint, Dark blue: ensemble  
 260 members satisfying the global temperature and total ice volume constraints, Red: ensemble members satisfying southern  
 261 North American ice sheet margin constraints in addition to global temperature and total ice volume constraints.

### 262 2.3 Integration procedure

263 Model simulations are all initiated from a static, isothermal (ice temperature 253 K) ice sheet and bedrock topography of  
 264 21ka BP of GLAC-1D (Fig. 3a, f, Tarasov et al. 2012). The simulations have two phases. First, there is an initial 5000 ice  
 265 sheet year spin-up with stand-alone BISICLES, where the ice sheet model parameter values are chosen according to the  
 266 ensemble Latin Hypercube sampling, but the associated climate parameter values are not used because there is no climate  
 267 model. In place of the climate model, a constant-in-time surface mass balance (*smb*, Table 1) and atmospheric surface  
 268 temperature of 253K are applied uniformly over the ice. Note that the ice temperature is allowed to evolve in the simulation.  
 269 The *smb* value is varied across the ensemble to produce a variety of total ice volumes (Fig. S1), because total ice volume is  
 270 highly uncertain in reconstructions and could be important given the dependence of ice sheet simulation on initial conditions  
 271 (Abe-Ouchi et al. 2013). The spin-up phase also gives the ice sheet model physics time to adjust from the prescribed initial  
 272 condition, i.e. it allows BISICLES to smooth out the blocky surface of the ice sheet reconstruction, providing some stability  
 273 to the simulations when they are subsequently coupled to the climate (FAMOUS) in the second phase. By the end of the  
 274 spin-up phase, 200 unique ice sheets have been modelled, providing the starting condition for simulations with BISICLES  
 275 coupled to FAMOUS in the second phase. In FAMOUS-BISICLES, *smb* is redundant and the climate parameters chosen by  
 276 Latin Hypercube are used in FAMOUS, with the same ice sheet parameter combinations as in the spin-up phase. In the  
 277 second phase, the simulations run another 5000 ice sheet (500 climate) years, which is insufficient to reach a quasi-  
 278 equilibrium state, but sufficiently long to see the effects of important parameters on the climate and ice sheets. For some of  
 279 the best performing simulations, the integration is extended for another 5000 ice years. However, the configuration of the ice  
 280 sheet showed only modest further changes (Fig. S2).



281  
 282 Fig. 3 Spatial maps of the initial condition for the ice sheet model, and results from the FAMOUS-BISICLES ensemble after  
 283 5000 ice sheet years. (a) ice topography [m] and (f) bedrock topography [m] from Tarasov et al. (2012). (b-e/top)  
 284 maps of surface altitude [m] and (g-j/bottom) surface mass balance [m/year] from ensemble means. (b, g) 87 members



285 satisfying the global mean temperature constraint, (c, h) 47 members satisfying both global mean temperature and ice  
286 volume constraints, (d, i) 16 members having the largest southern extent of North American ice sheet that satisfies  
287 temperature and volume constraints and (e, j) the member with most extensive southern ice area in the ensemble simulations.  
288 The thin black contour corresponds to the modern coastline, whereas the thick black contour in (g-j) corresponds to the zero  
289 line of SMB. Red contours in (a)-(e) correspond to the ice extent of Dalton et al. (2020). Black rectangle in (a) shows the  
290 region where the southern extent of the North American ice sheet is calculated (e.g. Fig. 11).

## 291 2.4 Constraints

292 Three metrics are used to evaluate the large-scale feature of the ensemble simulations. These are the annual mean LGM  
293 global surface air temperature, total ice volume of the North American and Greenland ice sheets and the southern extent of  
294 the North American ice sheet.

295

296 For the global temperature, we create our LGM constraint by adding estimates of the LGM global cooling to the  
297 Preindustrial global temperature. The Preindustrial temperature is 13.7 °C (1880-1900, NOAA National Centers for  
298 Environmental Information (2023)) with an uncertainty of  $\pm 0.1^\circ\text{C}$  (one standard deviation of global temperature during this  
299 period). According to previous studies, the LGM global cooling relative to the Preindustrial has a range of  $-1.7^\circ\text{C}$  to  $-8.3^\circ\text{C}$   
300 (e.g.,  $-1.7^\circ\text{C}$  to  $-3.7^\circ\text{C}$  with a probability of 90% in Schmittner et al. (2011) and  $-4.6^\circ\text{C}$  to  $-8.3^\circ\text{C}$  with a probability of 90% in  
301 Holden et al. (2010), see Fig. 4a in Tierney et al. 2020). Assuming the LGM cooling is normally distributed, this gives a  
302 mean cooling of  $5^\circ\text{C} \pm 3.3^\circ\text{C}$  with a probability of 90% (one standard deviation is  $\pm 2.0^\circ\text{C}$ ). Combining the uncertainties  
303 associated with the Preindustrial global temperature and the LGM global cooling gives one standard deviation of the  
304 uncertainty of

$$305 \sqrt{(0.1)^2 + (2.0)^2} = \pm 2.0^\circ\text{C}$$

306 in the actual LGM temperature (66% probability). To be conservative and take into account model uncertainty, we apply  
307 three standard deviations ( $\pm 6.0^\circ\text{C}$ ) as the uncertainty ranges. This gives an actual LGM temperature of approximately 2.7  
308 °C to 14.7 °C ( $8.7^\circ\text{C} \pm 6.0^\circ\text{C}$ ), with a probability of at least 99% (Pukelsheim 1994).

309

310 For the total ice volume constraint, previous studies have suggested that the volume of the North American ice sheet was  
311 likely to be higher than 60 m sea level equivalent (c.f. Abe-Ouchi et al. 2015). To account for model uncertainty and to be  
312 conservative, we apply a minimum reasonable North American ice volume of 50 m SLE as a constraint.

313

314 The southern extent of the North American ice sheet is used to select the best performing simulations, rather than as a strict  
315 constraint, because all ensemble members show a smaller southern area of the ice sheet than reconstructions (see Section  
316 4.1). Areas of grid cells covered by the ice sheet in the box shown in Fig. 3a are calculated. Simulations with the southern  
317 area covering 60% of the reconstruction (Dalton et al. 2020) are considered to satisfy our constraint.

318

319 In the end, sixteen simulations simultaneously satisfy our constraints on temperature, ice volume and extent.

## 320 3. Results

### 321 3.1 Response of the Global temperature

322 Fig. 4 summarises the temporal evolution of annual mean global mean temperature in the ensemble of simulations. After the  
323 first 300 ice sheet years, climates reach a quasi-equilibrium. The results show a wide variety of simulated global

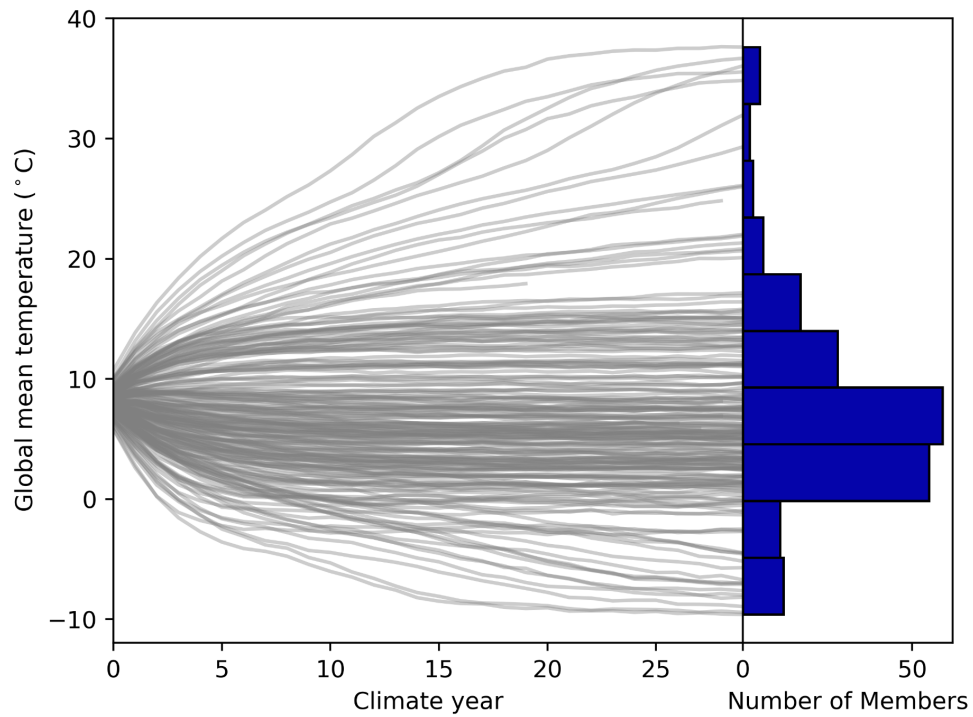


324 temperatures, ranging from  $-10^{\circ}\text{C}$  to  $40^{\circ}\text{C}$ . Such a wide range is frequently observed under parameter ensemble simulations  
325 (e.g. Joshi et al. 2010, Gregoire et al. 2011). The diverse response of global temperature is largely explained by two  
326 parameters in the cloud schemes;  $ct$  in the large-scale condensation scheme and  $entcoef$  in the cumulus convection scheme  
327 (Fig. 5). The correlation coefficients of these parameters with the global temperature at ice years 200-290 are 0.622 for  $ct$   
328 and  $-0.574$  for  $entcoef$ , respectively. In contrast, other parameters appear to have a smaller effect, according to the correlation  
329 analysis (Fig. 5). For the sea ice albedo, this relatively muted sensitivity may be related to the use of a slab ocean model,  
330 which underestimates the strong interactions between sea ice and oceanic heat transport over the Southern Ocean that  
331 amplifies the surface cooling at high latitudes (Ogura et al. 2004, Zhu et al. 2021). Including a dynamical ocean may increase  
332 the importance of sea ice albedo on the global temperature, as shown by Gregoire et al. (2011).

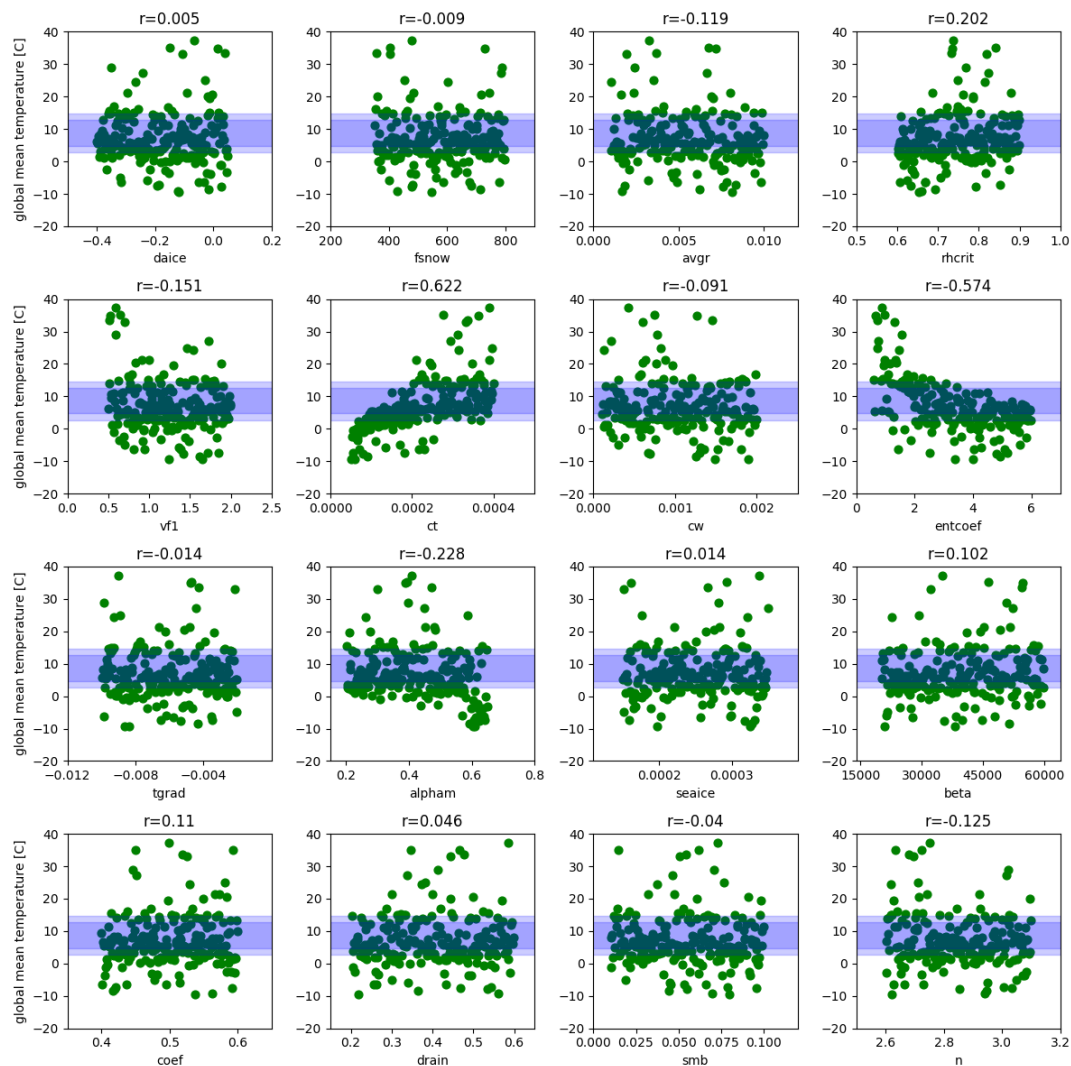
333

334 Roles of  $ct$  and  $entcoef$  in governing global temperature are further explored by means of a pair plot in Fig. 6. This figure  
335 compares the relationship of these two parameters to global temperature. The results show a positive correlation between  
336 global-scale warming and  $ct$ , which is associated with an increase in precipitation efficiency, reducing the life cycle of mid-  
337 latitude clouds, causing a decrease in the cloud cover and a decrease in the planetary albedo. As a result, more shortwave  
338 radiation is absorbed and the planet warms (Joshi et al. 2010, Sherriff-Tadano et al. 2023). Conversely, global-scale  
339 warming occurs with decreasing  $entcoef$  (Fig. 6), as the entrainment rate of ambient dry air in the tropics reduces, and the  
340 vertical transport of moisture to the high troposphere and lower stratosphere enhances. The planet then warms up due to the  
341 strong greenhouse gas effect of the water vapour (Joshi et al. 2010). Similar responses are observed in Joshi et al. (2010),  
342 who performed ensemble simulations under modern and future climates and showed that low values of  $entcoef$  were  
343 unrealistic based on the amount of water vapour in the lower stratosphere. Consistently, ensemble members with very low  
344 values of  $entcoef$  are more likely to be ruled out for producing implausible global mean temperatures, depending on the  
345 effect of the combinations of the other parameters (Fig. 6). For ensemble members satisfying the temperature constraint  
346 (black outlined coloured dots in Fig. 6), the overall cooling and warming effects of  $ct$  and  $entcoef$  are largely cancelled out  
347 by each other.

348



349  
350 Fig. 4 Evolution of global mean annual temperature in the Famous-Bisicles ensemble of simulations. Each grey line  
351 represents one ensemble member. Results from the first 300 ice years (30 climate years) are shown. Histograms on the right  
352 show the number of simulations in each temperature bin.  
353  
354



355

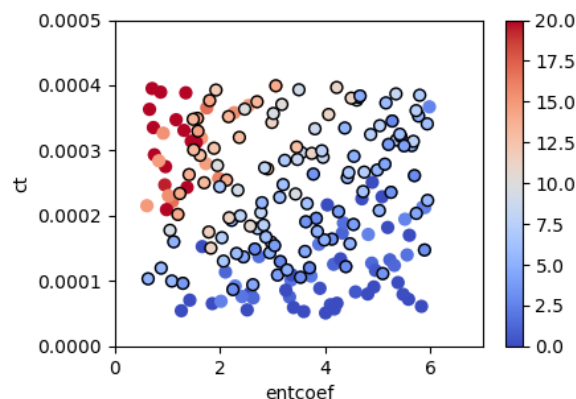
356

357

358

359

Fig. 5 Relationship between global mean temperature averaged over ice years 200-290 (climate years 20-29) and each parameter value. Correlation values are displayed above each panel. The uncertainties in global mean annual surface air temperature is shaded blue (three standard deviations for light blue and two standard deviations for dark blue).

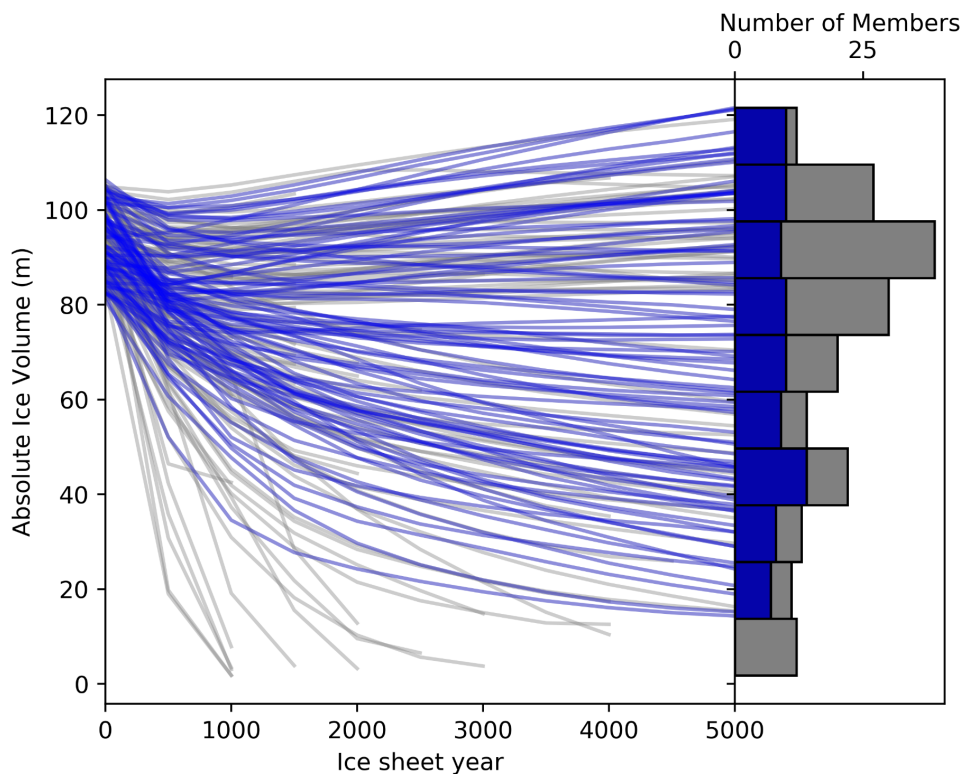


360

361 Fig. 6 Pair plot analysis exploring the combined effects of  $ct$  (precipitation efficiency in the large-scale condensation  
362 scheme) and  $entcoef$  (entrainment rate in the cumulus convection scheme) on global mean annual surface air temperature  
363 (colours, °C). Filled circles outlined in black are those satisfying the temperature evaluation criterion.

### 364 3.2 Response of the North American ice sheet and absolute ice volume

365 Similar to the diversity in simulated global mean temperature, the evolution of the ice sheet after the coupling to FAMOUS  
366 shows a wide range of responses (Fig. 7). Starting from absolute ice sheet volumes of 80 to 105 m SLE (sum of North  
367 American and Greenland ice sheets), the ensemble members produce absolute ice volumes between 0 and 120 m SLE at the  
368 end of the 5000-ice year integration. In some simulations, even the Greenland ice sheet disappears completely associated  
369 with the very high global temperature (Fig. 4). Note that some simulations with high  $n$  values or very warm climates (that  
370 cause all of the ice to rapidly disappear) crash during the integration. In total, 139 members (~ 70% of the ensemble)  
371 complete the entire 5000 ice years. Eighty-seven members satisfy the global temperature constraint (Fig. 5 and Fig. 6) , and  
372 47 members also satisfy the North American ice volume constraint of at least 50 m SLE. The additional constraint on the  
373 southern extent of the North American ice sheet selects the 16 best performing simulations (Fig. 2).



374  
375 Fig.7 Evolution of absolute ice volume of North America and Greenland in the FAMOUS-BISICLES LGM ensemble. Note  
376 that the ice volume of the entire Greenland is included. Each grey line represents one ensemble member. Blue lines are the  
377 members satisfying our chosen global temperature evaluation criteria. Histograms on the right show the number of  
378 simulations in each temperature bin; grey: all members and blue: members satisfying the global temperature constraint.

379

380 To explore which parameters are causing the variety of outcomes for the simulated North American ice volume, scatter plot  
381 and correlation analyses are performed (Fig. 8). Here, the ensemble members that both satisfy the global temperature  
382 constraint and have completed 5000 ice years are used (87 members). The analysis shows important impacts from  
383 parameters in our ice sheet surface albedo scheme that have a direct influence on the albedo that is diagnosed for bare ice or  
384 uncompacted snow surfaces; *avgr* (snow ageing effect), *daice* (melt pond effect), and *fsnow* (the weighting of snow and ice  
385 albedo based on the density of snow) showing correlations of -0.56, -0.475 and 0.372, respectively, with ice volume (see  
386 Table 1 for the effects of each parameter). Similar results are obtained for the analysis on the southern extent of the North  
387 American ice sheet (Fig. S4).

388

389 Additional analysis exploring the combined effect of these three parameters reveals a strong dependence between *daice* and  
390 *fsnow* (Fig. S7); the ice volume is less sensitive to *daice* when *fsnow* has a large value. This is reasonable as a large value of  
391 *fsnow* means that most of the snow/ice will be diagnosed as snow due to the high value of density threshold. As a result, the  
392 darkening effect for the old ice (*daice*) has only a minor influence.

393

394 The effects of other climate parameters are weaker compared to those of albedo parameters. Among these, *ct* shows the  
395 largest correlation value of -0.325. This is reasonable since the low value of *ct* corresponds to a colder global climate (Fig.





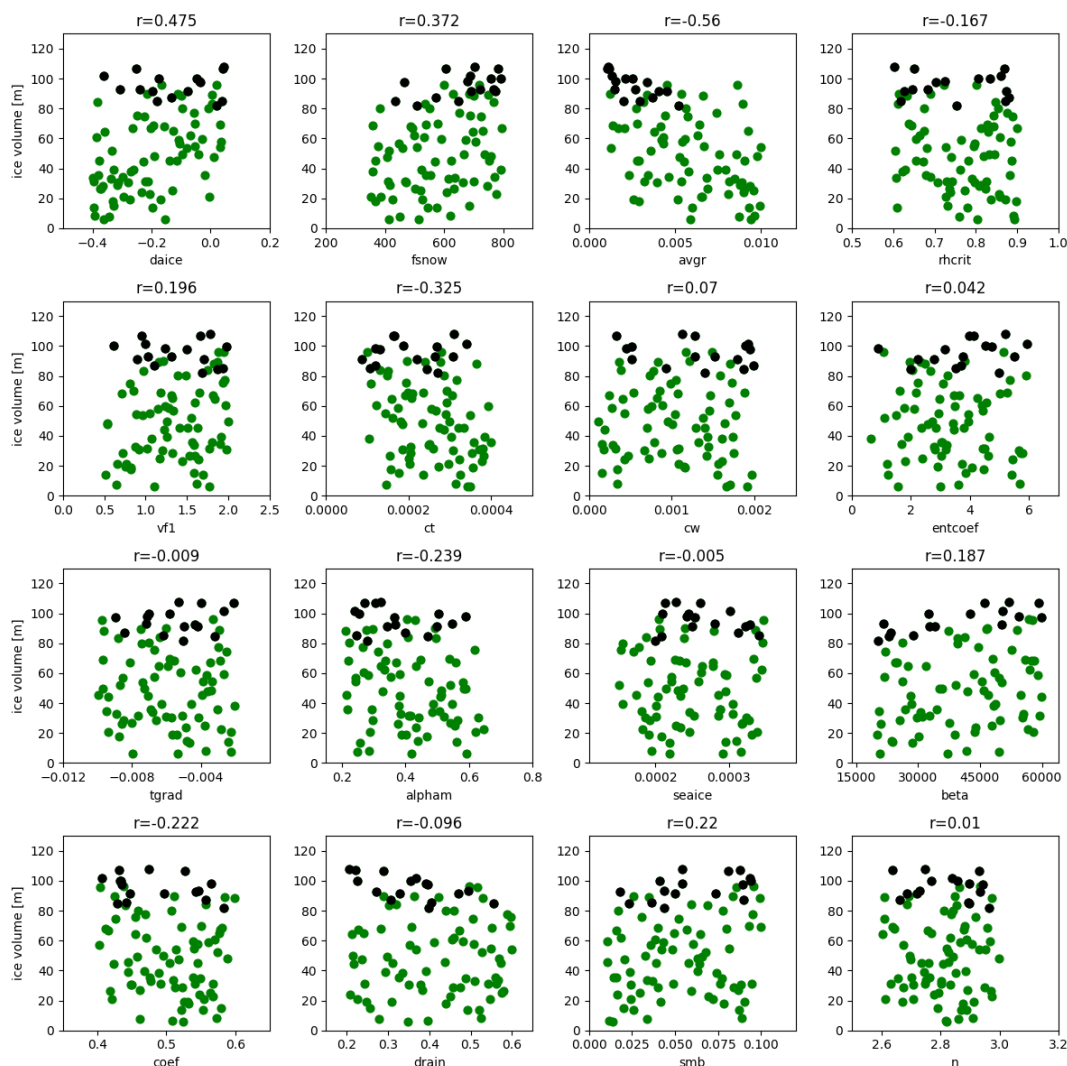
396 5), hence a colder local climate over the ice sheet, allowing the large ice sheet to be sustained (see also section 3.4 and Fig.  
397 11). On the other hand, the 87 not-ruled-out-yet simulations are relatively insensitive to *entcoef* (Fig. 8). This may in part be  
398 due to the screening out effect of ensemble members with low values of *entcoef* that causes drastically warm climates. We  
399 should also note that the cloud parameters exert some local influences on accumulation patterns, e.g. over the Gulf stream  
400 region (Fig. S6); larger values of *ct* and *cw* correspond to an increase in the amount of snowfall in this area. However the  
401 overall low correlation values between *cw* and the ice volume of North America shows a relatively weak effect of  
402 accumulation on the simulated ice volume.

403

404 Correlation analysis shows a very weak effect from basal drag parameters (*beta* and *coef*) on the ice volume (Fig. 8) and the  
405 southern extent (Fig. S4). The correlation value of *smb*, which controls the initial ice volume when the coupled climate-ice  
406 sheet phase of each simulation starts, is also low ( $r=0.22$ ). This suggests only a weak connection between final ice sheet  
407 volume at 5000 years and its initial volume at the beginning of the coupled simulations. This is due to the large  
408 modifications in snow/ice albedo in our ensemble design, which is capable of drastically altering the magnitude of absorbed  
409 solar radiation over the ice sheet (e.g. Abe-Ouchi et al. 2013). For other dynamical ice sheet parameters (*drain* and *n*), the  
410 correlations are generally even lower. Overall, the North American ice sheet volume is much less sensitive to uncertainty in  
411 ice sheet dynamics than ice sheet albedo and climate in our parameter space.

412

413 Interestingly, we find that the main results showing the importance of albedo parameters can be found in the first 500 ice  
414 sheet years by analysing the relation of ice volume changes and each parameter (106 members, Fig. S3). Similar results are  
415 also obtained by Gregory et al. (2020), who show that the SMB of the first 100 years can be a good predictor of the final  
416 steady state ice sheet mass of modern and future Greenland. These results suggest that significant computational cost could  
417 be saved for at least an initial exploration of model sensitivity to uncertain parameter values (e.g. if designing a multi-wave  
418 ensemble experiment).



419

420 Fig. 8 Relationship between North American ice volume at 5000 ice years in FAMOUS-BISICLES and each perturbed  
 421 parameter. Only those ensemble members that satisfy the global temperature constraint are used. Correlation values are  
 422 displayed above each panel. Black dots correspond to the best sixteen members.

423

424 To explore our preferred parameter space that produces good climate and ice sheets at the LGM, the distributions of  
 425 parameters satisfying the applied constraints are examined (Fig. 2). Results show that some of the parameter ranges may be  
 426 ruled out due to poor resulting simulation performance, such as values below 400 of *fsnow*, values above 0.006 of *avgr*,  
 427 values below 0.00008 of *ct* and values above 3.0 of *n*. Additionally, from Fig. S7, a combination of low values in both *daice*  
 428 and *fsnow* may be ruled out. Runs that satisfy the constraints tend to have parameters that lead to higher albedo values. For  
 429 other parameters, it is shown that values across any individual parameter range in the ensemble can produce reasonable  
 430 global temperatures and ice sheets, depending on their combination with others.

431

432 The performance of the simulated ice extent in the best sixteen simulations (Fig. 3d) is further evaluated against the ice  
 433 extent reconstruction from Dalton et al. (2020, red contour in Fig. 3d). In general, the average of the best sixteen simulations



434 reproduces the overall ice extent of the North American ice sheet reasonably well; e.g. performances over the northern  
435 margin and the southern margin west of 110°W and east of 80°W are reasonable. Also the performance is much better  
436 compared to means of members that satisfies the global temperature and the ice volume constraints (Fig. 3b, c). In contrast,  
437 the main differences between the best sixteen simulations and the reconstruction appear over the southern margin at 110°W -  
438 80°W, where the model underestimates the area of the ice sheet. Another difference can be found over Alaska, where the  
439 model overestimates the ice sheet area and thickness (Fig. 3d). These features are commonly observed in ice sheet model  
440 simulations coupled to a low-resolution atmospheric model and will be discussed in section 4.1.

441

442 Away from the southern margin, the best performing FAMOUS-BISICLES simulations tend to lack sufficient ice at the  
443 eastern margin, where an ice shelf should exist (Fig. 3d). This is associated with the strong and uniform basal ice shelf  
444 melting applied in this study. The basal melting around the coastal area largely depends on the configuration of the  
445 continental shelf as well as the ambient ocean temperature, as shown by studies on the Antarctic ice sheet (e.g. Obase et al.  
446 2017). Future work could undertake additional sensitivity experiments changing the magnitudes and patterns of the basal  
447 melting to further explore this point.

### 448 3.3 Responses of the Greenland ice sheet

449 The Greenland ice sheet also shows various responses to modifications in the parameters in the ensemble of simulations,  
450 ranging from 8 m SLE to 15 m SLE (Fig. 9). The simulated range is similar to the range in the reconstructions suggesting  
451 9.3 m to 12.3 m SLE (7.3 m + 2~5 m SLE, Clark and Mix 2002, Lecavalier et al. 2014, Bradley et al. 2018, Tabone et al.  
452 2018), while the model overestimates the higher band.

453

454 Interestingly, the results show a different sensitivity to the model parameters we vary compared to the North American ice  
455 sheet (Fig. 9). The variations in the ice volume are mostly explained by changes in *beta*, where higher values increase the  
456 friction between the ice sheet and the bedrock at a cold ice base. This acts to increase the ice volume by reducing the amount  
457 of ice transported to its margin which then calves at the continental shelf, and hence by inducing thickening of the ice sheet  
458 interior.

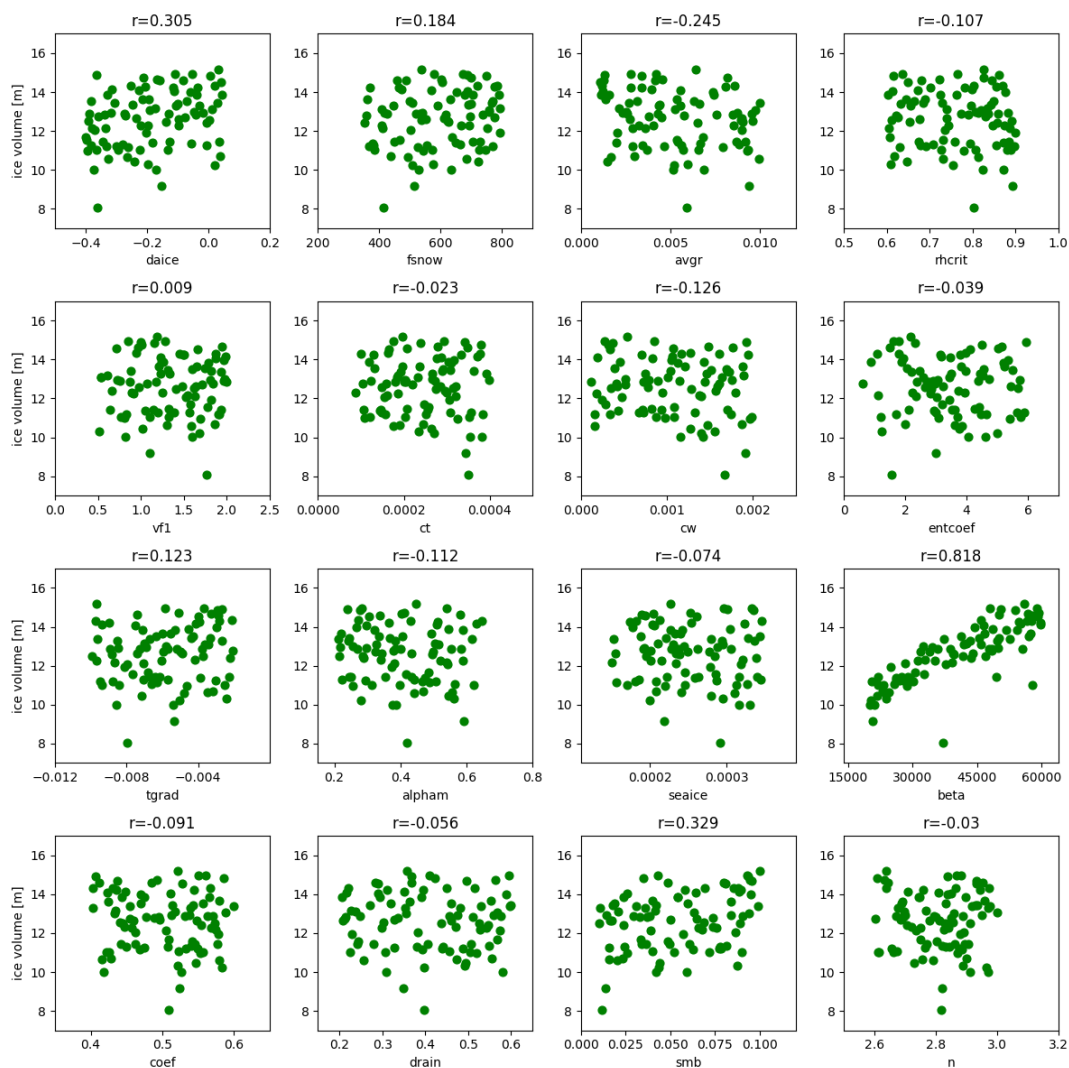
459

460 The lower sensitivity of the Greenland ice sheet to albedo parameters comes from different climatic conditions compared to  
461 North America. In North America, the large area is covered by negative surface mass balance (Fig. 3g) as the summer  
462 temperature can be close to freezing point in the simulations (Fig. 10). Hence, albedo parameters cause a drastic difference  
463 since they control the magnitude of the negative SMB over North America (Fig. 8). In contrast, the Greenland ice sheet is  
464 covered by colder conditions in summer (Fig. 10), hence most surface areas have positive surface mass balance (Fig. 9).  
465 Under this condition, the amount of the ice loss is determined by the amount of ice transported from the interior to its edge,  
466 which then calves. As a result, the ice volume is mainly driven by *beta* since it controls the transport of ice under the cold ice  
467 base.

468

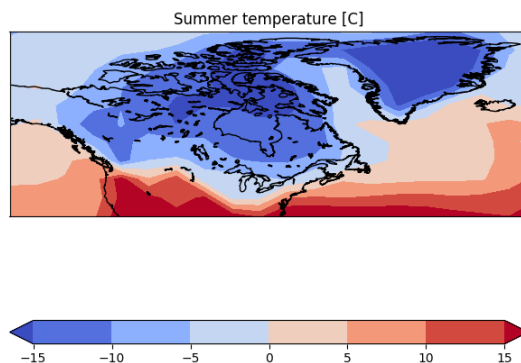
469 Previous studies have shown that basal melting of ice shelves by the underlying ocean is also important in controlling  
470 Greenland ice sheet volume at the LGM in their coupled ice shelf-ice sheet models (Bradley et al. 2018, Tabone et al. 2018).  
471 In this study, however, a constant value was given for the ice shelf basal melting. Conducting ensemble simulations with  
472 variations in the amount of ice shelf melting may enable us to explore the relative importance.

473



474

475 Fig.9 Relation of ice volume of Greenland at 5000 ice years in FAMOUS-BISICLES and each parameter. Ensemble  
 476 members satisfying the global temperature constraint are used. Correlation values are displayed on the top of each panel.



477



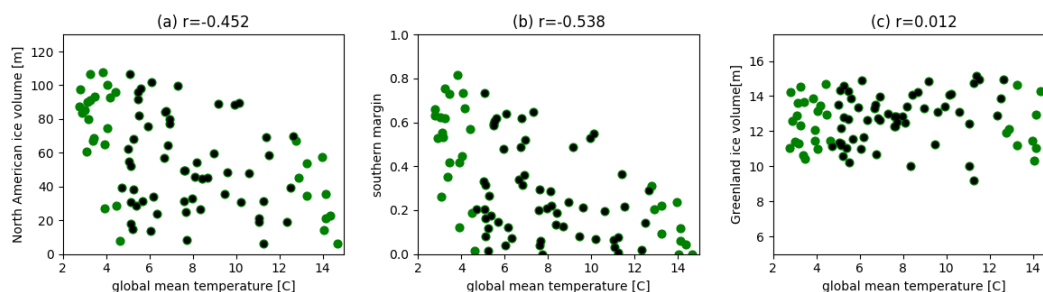
478 Fig.10 Summer surface air temperature [ $^{\circ}\text{C}$ ] over North America and Greenland, averaged over all ensemble members  
479 satisfying the global temperature constraint.

### 480 3.4 Effects of global mean temperature on ice sheet volume

481 The sensitivity of the ice sheets to the reasonable LGM global temperature range ( $2.7^{\circ}\text{C}$ - $14.7^{\circ}\text{C}$ ) is explored to see any  
482 possible relationship between them (Fig. 11). The results show a high correlation between the global temperature and North  
483 American ice volume/southern extent; colder climates correspond to larger and more extensive ice sheets (Fig. 11a, b). This  
484 is not a surprise since a large uncertainty of  $\pm 6.0^{\circ}\text{C}$  is applied to the global temperature. Reducing the uncertainty level to  
485 two sigma ( $8.7^{\circ}\text{C} \pm 4.0^{\circ}\text{C}$ , black dots in Fig. 11) weakens the correlation between the global temperature and the North  
486 American ice volume/southern extent to  $-0.193$  and  $-0.285$ , respectively. Nevertheless, the correlation analysis still shows  
487 some sensitivity of the southern extent of the North American ice sheet to global temperature (Fig. 11b), where a colder  
488 global climate tends to produce a more extensive ice sheet in the south. In other words, it can also be said that it is hard to get  
489 an extensive southern North American ice sheet under warm LGM global temperature (above  $12.0^{\circ}\text{C}$ ), irrespective of the  
490 albedo parameters, which demonstrates the value of constraining the upper band of real LGM temperatures for simulating  
491 the North American ice sheet well.

492

493 The Greenland ice sheet appears to be insensitive to the reasonable LGM global temperature range ( $2.7^{\circ}\text{C}$ - $14.7^{\circ}\text{C}$ ), which is  
494 consistent with the dominant role of basal sliding in controlling the ice volume. Reducing the uncertainty level to two sigma  
495 ( $8.7^{\circ}\text{C} \pm 4.0^{\circ}\text{C}$ , black dots in Fig. 11) increases the correlation value to  $0.259$  possibly associated with an increase in snow  
496 fall following the warming climate, however the effect is much weaker compared to the effect of basal sliding.



497

498 Fig. 11 Relationship between global mean annual surface air temperature [ $^{\circ}\text{C}$ ] and Ice sheet variables. (a) North American  
499 ice sheet volume [m], (b) Ratio of southern extent of the North American ice sheet compared to Dalton et al. (2020) and (c)  
500 Greenland ice sheet volume [m]. Ensemble members that satisfy the global temperature constraint and have run 5000 ice  
501 sheet years are used (87 members). Correlation values are also shown in each figure. Black dots show results within the two  
502 sigma uncertainty in the LGM global temperature ( $8.7^{\circ}\text{C} \pm 4.0^{\circ}\text{C}$ ).

## 503 4. Discussion

### 504 4.1 How could FAMOUS-BISICLES be made to reproduce the southern extent of the North American ice sheet?

505 A recent study by Gandy et al. (2023) performed a similar ensemble simulation with FAMOUS-GLIMMER with fixed SSTs  
506 instead of FAMOUS-BISICLES coupled to a slab ocean model used in this study. Our findings here are consistent with them  
507 in that the ice extent is sensitive to choices of parameters in the snow and ice albedo scheme and that both models  
508 underestimate the southern extent of the North American ice sheet, especially the so-called ‘lobe’ characteristics. To  
509 investigate the possibility of the model being able to reproduce the full extent of the southern margin of the North American



510 ice sheet, we analyse in detail the ensemble member that has the most extensive southern margin, disregarding our imposed  
511 climate plausibility constraints (Fig. 3e). In the simulation, the performance of the southern extent of the North American ice  
512 sheet improves and becomes closer to the reconstructed area due to the very cold climate, whose absolute global temperature  
513 is  $-7.4^{\circ}\text{C}$ . Yet even in this very cold simulation, the model cannot maintain the ‘lobe’ characteristics of the North American  
514 ice extent as far south as the reconstructions.

515

516 So, how might we reproduce the southern margin of the North American ice sheet? There are several possibilities:

- 517 • **Finer horizontal resolution in the climate model:** during the simulations, FAMOUS-BISICLES loses the thin ice  
518 sheet at the south margin abruptly in the first 1000 ice sheet years due to the very large negative SMB simulated in  
519 the atmospheric model (e.g. Fig. 13b). As discussed above, applying a high-resolution atmospheric model might be  
520 better able to sustain a more southerly ice margin through a stronger stationary wave effect that cools the area (Abe-  
521 Ouchi et al. 2007).
- 522 • **Representation of clouds:** Gregory et al. (2012) pointed out the importance of changes in cloud cover over the  
523 southern margin of the North American ice sheet on its SMB during the glacial inception. Having a larger cloud  
524 cover at the southern margin may help to maintain the ice sheet by reducing the very large negative SMB, while a  
525 careful analysis on the physical plausibility needs to be done.
- 526 • **Improvements in the downscaling scheme:** including the effect of strongly stratified boundary layer on the surface  
527 temperature during the downscaling may allow a colder surface temperature over ice, which can help sustain the ice  
528 sheet at its margin. Incorporation of downscaling of accumulation in FAMOUS-BISICLES can increase the snow  
529 fall at the southern margin, which increases the SMB and surface albedo and may help to sustain the ice sheet at the  
530 southern margin (e.g. Yamagishi and Abe-Ouchi 2005).
- 531 • **Higher initial surface elevation:** the simulation could be started with a higher initial surface elevation which can be  
532 obtained by giving a thicker ice or a higher bedrock topography at the southern margin, allowing for lower surface  
533 temperatures due to the higher elevation, although this may not be physically plausible.
- 534 • **Palaeo-vegetation:** the choice of vegetation type for the unglaciated region near to the ice sheet may be relevant.  
535 The modern vegetation distribution used in this study may tend to give a warmer condition in this area, unlike  
536 tundra, which grows under cold climates and causes a surface cooling (O’ishi and Abe-Ouchi 2013).
- 537 • **Bedrock conditions:** creating a slippery bedrock condition would enhance ice flow from the ice sheet interior  
538 towards the margin, and so may be instrumental in redistributing ice outwards.
- 539 • **Longer integration of the model:** extending the integration of FAMOUS-BISICLES may help to redistribute the  
540 thick ice in the interior to the southern margin. In fact, some of the members, which have been extended for  
541 additional 5000 years show a southward expansion (Fig. S2).

542 It is also possible that the concept of the southern margin being in a quasi-equilibrium state with the LGM forcing may not  
543 be valid, and that it may be reflecting several transient ice advancing events that occurred during the recent glacial period  
544 (and preceding the LGM)(e.g. Pico et al. 2017, Gowan et al. 2021, Bradley et al. 2023). We speculate that such earlier  
545 southward ice advance may allow a more expansive southern ice sheet to establish, before rebalancing with the insolation  
546 forcing. In this case, running a long transient simulation, rather than performing equilibrium-type LGM simulations, may be  
547 essential for achieving the target southern margin extent.

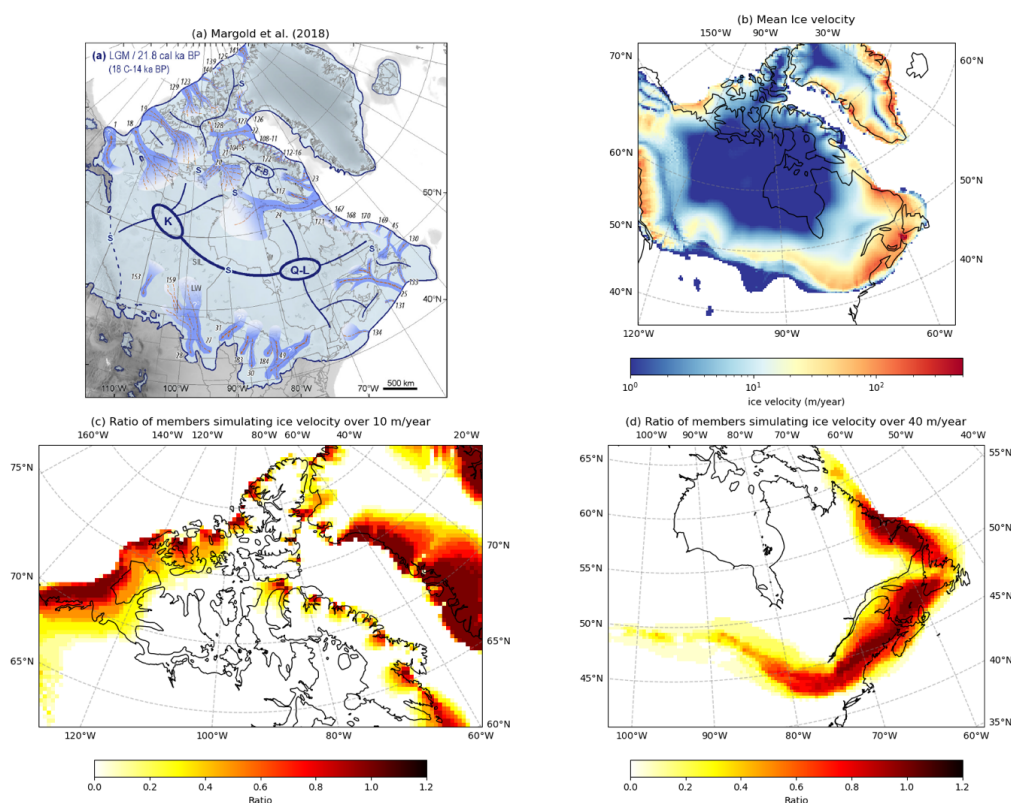
#### 548 **4.2 Performances of ice streams**

549 The positions of our simulated ice streams in the best sixteen ensemble members are evaluated against the reconstruction by  
550 Margold et al. (2018) (Fig. 12 and Fig. S5). The figure depicts that BISICLES shows regions of relatively high ice velocities  
551 (or ice streams) at various sites, despite the relatively low resolution of the model (16 km at finest grid) and the relatively





552 short integration period. Specifically, most members reproduce high ice velocities at the margin over the Baffin Bay area. In  
553 addition, the simulation of ice streams facing the Arctic Ocean is encouraging (Fig. 12, S5). However, once again the  
554 southern margin is tricky to get right, and our ice stream behaviour there is somewhat diffuse, not picking up the  
555 characteristic ‘lobe’ structure of the reconstructions (Margold et al. 2018). Over the Eastern North American ice sheet, the  
556 model captures some large glaciers such as Laurentian Channel (25), Placentia Bay-Halibut Channel (133) and Hopedale  
557 Saddle (168), while none of the best sixteen ensemble members simulate the large ice stream that flows to the Labrador Sea  
558 from the present-day Hudson Bay area. These poorly represented ice stream features may be caused by low resolution of the  
559 smallest ice sheet refinement (16 km, e.g. Gandy et al. 2019), too-short integration and misrepresentation of the surface type  
560 of till (Gowan et al. 2019). With the last point, the amount of till water calculated prognostically in the simulations appears  
561 small, hence most areas use the Weertman sliding law. An increase in the basal melting, a choice of a smaller value for  
562 *drain* or incorporating a spatially variable Weertman coefficient map based on geological evidence may help to improve the  
563 performance of the ice streams. Nevertheless, the model does show some reasonable potential in simulating North American  
564 ice streams considering the relatively low resolution as well as the explicit calculation of basal drag.  
565



566  
567 Fig.12 Comparison of ice velocity [m/year, colour] between (a) Reconstruction (Margold et al. 2018, adapted from Fig. 5 of  
568 Margold et al. 2018) and (b) the mean of best sixteen members. (c) and (d) show the ratio of numbers of members simulating  
569 ice velocity beyond 10m/year for (c) and 40m/year for (d), respectively. Ratio of 1.0 means all the sixteen members simulate  
570 ice velocities of those values.

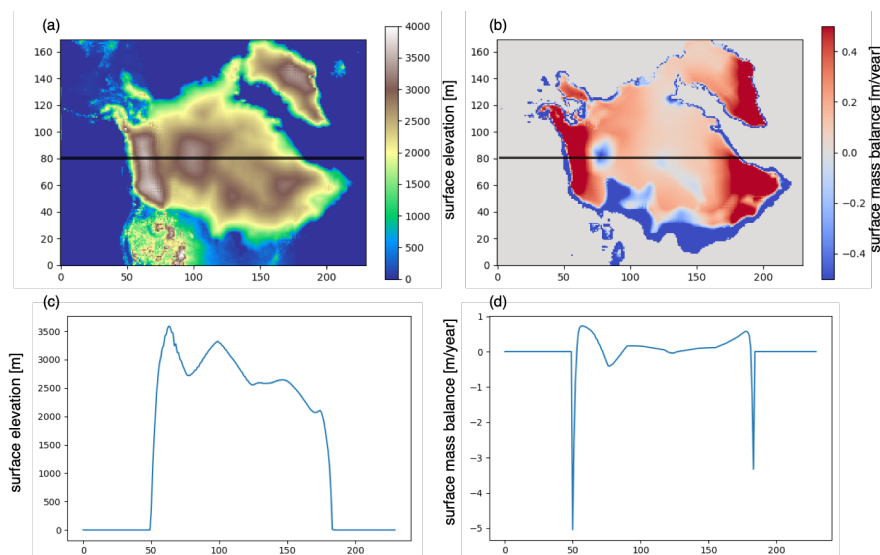
571 **4.3 Effects of biases in the simulated climate**





572 Some of the simulations in the ensemble exhibit a local melting of the ice sheet from parts of the interior outwards, which is  
573 unusual, as ice sheets usually melt from their margins, where the surface temperature is close to the freezing point (e.g. Figs  
574 3c and 13). This phenomenon is caused by biases in the atmospheric model, which are then amplified by the downscaling  
575 method and a positive feedback from the coupling. First, the model has a warm summer temperature bias over the ice sheet  
576 interior. As a result, large parts of the central North American ice sheet have a temperature above  $-10^{\circ}\text{C}$  despite the surface  
577 elevation exceeding 2000 m (Fig. 10). A similar feature was pointed out by Smith et al. (2021) using the same model under  
578 the modern Greenland ice sheet, which produced a higher ELA (around 2 km high) compared to a high resolution regional  
579 atmospheric model (at about 1 km high). Second, because the downscaling of SMB strongly depends on the elevation, a  
580 local change in surface elevation can induce a local negative surface mass balance if the surface temperature calculated in the  
581 FAMOUS grid points are close to the freezing point. This example is shown in Fig. 13, where a negative SMB can be found  
582 at the local minimums of surface elevation, despite the elevation exceeding 2000 m. The initial negative SMB then kicks in a  
583 strong positive feedback where melting of snow reduces the albedo and results in more energy absorption. As a result, the ice  
584 elevation starts to decrease and causes additional positive feedback similar to saddle node collapse (Gregoire et al. 2012).  
585 This way of downscaling the climate model output works well for modern Greenland, especially at low elevation where the  
586 SMB has very strong elevation dependence. However, at the higher altitudes achieved by the LGM North American ice  
587 sheet, SMB may be more greatly affected by other factors such as wind speeds, as suggested by studies on Antarctica (Van  
588 Liefferinge et al. 2021). Hence, further improvements in the downscaling method at higher elevation could help to reduce the  
589 impact of the climate biases.

590



591

592 Fig.13 An example of local ice melting in the interior of the ice sheet. (a) Surface topography [m] and (b) Surface mass  
593 balance [m/year]. Height zonal cross-section of (c) surface topography and (d) surface mass balance at  $y=80$  are shown.

## 594 5. Conclusion

595 In this paper we have presented a large ensemble of simulations of the North American and Greenland ice sheets and climate  
596 of the LGM, performed with a coupled atmosphere-ice sheet-slab ocean model FAMOUS-BISICLES, a version of the  
597 FAMOUS-ice model developed by Smith et al. (2021). The experiment consists of a 200-member perturbed parameter  
598 ensemble, where the values of 16 parameters associated with climate and ice dynamics were varied using a Latin-hypercube  
599 sampling method. The simulated results are evaluated against the LGM global mean surface air temperature, the North



500 American ice volume and the southern extent of the North American ice sheet. In the ensemble, the global temperature is  
501 controlled by a combination of precipitation efficiency in the large-scale condensation and entrainment rate in the cumulus  
502 convection, consistent with previous FAMOUS simulations of modern climate (Joshi et al. 2010). Under reasonable LGM  
503 global temperature conditions, we find that the surface albedo exerts the strongest control on North American ice volume. In  
504 contrast, the ice volume of Greenland is found to be mainly controlled by the Weertman coefficient in the basal sliding law.  
505 The different sensitivity of these ice sheets to the model's physical parameter values mainly comes from different climatic  
506 conditions; the North American ice sheet being generally warmer hence has a larger area of negative SMB, which is affected  
507 by the albedo. In contrast, most parts of the Greenland ice sheet are covered by a very cold atmosphere, hence the ice sheet  
508 volume is more affected by the calving at its margin, the total amount of which is controlled by the magnitude of the basal  
509 sliding law that affects the amount of ice transported to the margins. These differences between the North American and  
510 Greenland ice sheets provide an important take-home message on model performance, suggesting that for best flexibility  
511 (i.e., the ability to simulate conditions largely different from today), simulators should be calibrated under substantially  
512 different climate and ice sheet conditions and tested out-of-sample.

513

514 Analysis of the relationship between the North American southern ice extent and global temperature with the uncertainty  
515 level of two sigma ( $8.7^{\circ}\text{C} \pm 4.0^{\circ}\text{C}$ ) shows a slightly weak relation. Nevertheless, we find that it is hard to get an extensive  
516 southern North American ice sheet under warm LGM global temperature (above  $12.0^{\circ}\text{C}$ ), irrespective of the albedo  
517 parameters in our model. This demonstrates the value of constraining the upper band of real LGM temperatures for  
518 simulating the North American ice sheet well.

519

520 Based on our plausibility constraints, the model produces sixteen 'acceptable' simulations with reasonable global  
521 temperature and North American ice sheet. These simulations show the most extensive southern margin under reasonable  
522 LGM temperature and ice volume, but, as with many LGM ice sheet simulations, are not sufficiently expansive at the  
523 southern margin and overestimate ice volume in Alaska. Both of these features are likely attributable to the underestimation  
524 of the stationary wave effect (Roe and Lindzen 2001, Abe-Ouchi et al. 2007), and may be improved upon/overcome by  
525 increasing the climate model resolution. We find that the model cannot reproduce the southern margin of the ice sheet over  
526 the 5000-year simulation even if the absolute global temperature is as cold as  $-7.4^{\circ}\text{C}$ , and it is also possible that more  
527 accurate representation of the palaeo vegetation, different treatments of ice sheet sliding and downscaling method of the  
528 SMB, or a different spin-up procedure could improve the simulated southerly ice sheet extent.

529

530 Our results show that warm summer temperature biases in the interior of the ice sheet as well as the downscaling method of  
531 SMB based on elevation can cause strong local melting of the ice sheet from the interior outwards. More complex treatment  
532 of the atmospheric conditions and surface mass balance in the ice sheet interior could improve this, and may be especially  
533 important when applying the model to the Antarctic ice sheet.

534

535 Lastly, the strong sensitivities of the North American ice sheet to albedo at the LGM may imply a potential constraint on the  
536 future Greenland ice sheet by constraining the formulation and behaviour of albedo schemes for climate and ice sheet models  
537 under relatively warm climates. Running similar ensemble simulations for the modern and future Greenland ice sheet will  
538 provide an important data set to directly connect the simulations of past climates and ice sheets to those of the modern and  
539 future. Using such data, we may be able to explore whether simulations of past climate-ice sheet conditions can more tightly  
540 constrain or increase the confidence of projection of future sea level rise .

541 **Code and data availability**



542 The simulation data of FAMOUS-BISICLES used in this study will be available in a public database.

#### 543 **Author contribution**

544 Sam Sherriff-Tadano (Data curation, Formal Analysis, Investigation, Methodology, Validation, Visualization, Writing-  
545 original draft), Ruza Ivanovic (Conceptualisation, Funding Acquisition, Investigation, Methodology, Project Administration,  
546 Resources, Software, Supervision, Writing - review and editing), Lauren Gregoire (Conceptualisation, Funding Acquisition,  
547 Investigation, Methodology, Project Administration, Resources, Software, Supervision, Writing - review and editing),  
548 Charlotte Lang (Data curation, Formal Analysis, Investigation, Methodology, Writing-review and editing), Niall Gandy  
549 (Data curation, Formal Analysis, Investigation, Methodology, Writing-review and editing), Tamsin Edwards (Funding  
550 acquisition, Methodology, Writing – original draft). Robin S. Smith (Conceptualisation, Funding Acquisition, Methodology,  
551 Project Administration, Resources, Software, Supervision, Writing - review and editing), Jonathan Gregory  
552 (conceptualization, funding acquisition, methodology, software, writing - review and editing), Oliver Pollard (Methodology,  
553 Visualization, Writing - review and editing)

#### 554 **Competing interest**

555 The authors declare no competing interests.

#### 556 **Acknowledgements**

557 This work was undertaken on ARC4, part of the High Performance Computing Facilities at the University of Leeds,  
558 ARCHER2 and JASMIN. RFI, RSS, JG, TE, CL and SST were funded by “RiSICMAP”, NERC Standard Grant  
559 NE/T007443/1. NG, LJG, RFI were funded by “SMB-Gen” UKRI Future Leaders Fellowship MR/S016961/1. We are also  
560 grateful to Richard Rigby for his assistance in setting up the simulation. SST also thanks Ayako Abe-Ouchi, Miren Vizcaino,  
561 Heiko Goelzer and Jonathan Owen for constructive discussion.

#### 562 **References**

- 563 Abe-Ouchi, A., et al.: Ice-sheet configuration in the CMIP5/PMIP3 Last Glacial Maximum experiments. *Geoscientific*  
564 *Model Development*, 8, 3621-3637. <https://doi.org/10.5194/gmd-8-3621-2015>, 2015.
- 565 Abe-Ouchi, A., et al.: Insolation-driven 100,000-year glacial cycles and hysteresis of ice-sheet volume. *Nature*, 500, 190-+.  
566 <https://doi.org/10.1038/nature12374>, 2013.
- 567 Abe-Ouchi, A., Segawa, T., & Saito, F.: Climatic Conditions for modelling the Northern Hemisphere ice sheets throughout  
568 the ice age cycle. *Climate of the Past*, 3, 423-438. <https://doi.org/10.5194/cp-3-423-2007>, 2007.
- 569 Alder, J.R., Hostetler, S.W.: Applying the Community Ice Sheet Model to evaluate PMIP3 LGM climatologies over the  
570 North American ice sheets. *Clim Dyn* 53, 2807–2824. <https://doi.org/10.1007/s00382-019-04663-x>, 2019.
- 571 Blasco, J., Alvarez-Solas, J., Robinson, A., and Montoya, M.: Exploring the impact of atmospheric forcing and basal drag on  
572 the Antarctic Ice Sheet under Last Glacial Maximum conditions, *The Cryosphere*, 15, 215–231.  
573 <https://doi.org/10.5194/tc-15-215-2021>, 2021.
- 574 Braconnot, P. et al.: Evaluation of climate models using palaeoclimatic data. *Nature Climate Change* 2, 417-424.  
575 <https://doi.org/10.1038/nclimate1456>, 2012.
- 576 Braconnot, P. et al.: Results of PMIP2 coupled simulations of the Mid-Holocene and Last Glacial Maximum - Part 1:  
577 experiments and large-scale features. *Climate of the Past* 3, 261-277. 2007.
- 578 Bradley, S. L., Reerink, T. J., van de Wal, R. S. W., and Helsen, M. M.: Simulation of the Greenland Ice Sheet over two  
579 glacial–interglacial cycles: investigating a sub-ice- shelf melt parameterization and relative sea level forcing in an ice-  
580 sheet–ice-shelf model, *Clim. Past*, 14, 619–635. <https://doi.org/10.5194/cp-14-619-2018>, 2018.
- 581 Bradley, S. L., Sellevold, R., Petrini, M., Vizcaino, M., Georgiou, S., Zhu, J., Otto-Bliesner, B. L., and Lofverstrom, M.:  
582 Surface mass balance and climate of the Last Glacial Maximum northern hemisphere ice sheets: simulations with



- 583 CESM2.1, *Clim. Past Discuss.* [preprint], <https://doi.org/10.5194/cp-2023-62>, in review, 2023.
- 584 Briggs, R. D., Pollard, D., and Tarasov, L.: A data-constrained large ensemble analysis of Antarctic evolution since the  
585 Eemian, *Quatern. Sci. Rev.*, 103, 91–115. <https://doi.org/10.1016/j.quascirev.2014.09.003>, 2014.
- 586 Clark, P. U. et al.: The Last Glacial Maximum. *Science* 325, 710-714. <https://doi.org/10.1126/science.1172873>, 2009.
- 587 Clark, P. U. and Mix, A. C.: Ice sheets and sea level of the Last Glacial Maximum, *Quaternary Science Reviews*, Volume  
588 21, Issues 1–3, 2002, Pages 1-7. [https://doi.org/10.1016/S0277-3791\(01\)00118-4](https://doi.org/10.1016/S0277-3791(01)00118-4), 2002.
- 589 Cornford, S. L., Martin, D. F., Graves, D. T., Ranken, D. F., Le Brocq, A. M., Gladstone, R. M., Payne, A. J., Ng, E. G.,  
590 Lipscomb, W. H.: Adaptive mesh, finite volume modeling of marine ice sheets, *Journal of Computational Physics*,  
591 Volume 232, Issue 1, 2013, Pages 529-549. <https://doi.org/10.1016/j.jcp.2012.08.037>, 2013.
- 592 Dalton, A. S. et al.: An updated radiocarbon-based ice margin chronology for the last deglaciation of the North American Ice  
593 Sheet Complex, *Quaternary Science Reviews*, Volume 234, 106223, ISSN 0277-3791,  
594 <https://doi.org/10.1016/j.quascirev.2020.106223>, 2020.
- 595 DeConto, R., Pollard, D.: Contribution of Antarctica to past and future sea-level rise. *Nature* 531, 591–597.  
596 <https://doi.org/10.1038/nature17145>, 2016.
- 597 Dyke, A.S. et al.: The Laurentide and Innuitian ice sheets during the Last Glacial Maximum, *Quaternary Science Reviews*,  
598 Volume 21, Issues 1–3, Pages 9-31, ISSN 0277-3791, [https://doi.org/10.1016/S0277-3791\(01\)00095-6](https://doi.org/10.1016/S0277-3791(01)00095-6), 2002.
- 599 Edwards, T. L. et al.: Projected land ice contributions to twenty-first-century sea level rise. *Nature* 593, 74+.  
700 <https://doi.org/10.1038/s41586-021-03302-y>, 2021.
- 701 Gandy, N. et al.: Marine ice sheet instability and ice shelf buttressing of the Minch Ice Stream, northwest Scotland.  
702 *Cryosphere* 12, 3635-3651. <https://doi.org/10.5194/tc-12-3635-2018>, 2018.
- 703 Gandy, N. et al.: Exploring tile ingredients required to successfully model the placement, generation, and evolution of ice  
704 streams in the British-Irish Ice Sheet. *Quaternary Science Reviews* 223.  
705 <https://doi.org/10.1016/j.quascirev.2019.105915>, 2019.
- 706 Gandy, N., Astfalek, L. C., Gregoire, L. J., Ivanovic, R. F., Patterson, V. L., Sherriff-Tadano, S., et al.: De-tuning albedo  
707 parameters in a coupled Climate Ice Sheet model to simulate the North American Ice Sheet at the Last Glacial  
708 Maximum. *Journal of Geophysical Research: Earth Surface*, 128, e2023JF007250.  
709 <https://doi.org/10.1029/2023JF007250>, 2023.
- 710 Gолledge, N. R. et al.: Global environmental consequences of twenty-first-century ice-sheet melt. *Nature* 566, 65+.  
711 <https://doi.org/10.1038/s41586-019-0889-9>, 2019.
- 712 Gowan, E. J. et al.: A new global ice sheet reconstruction for the past 80000 years. *Nature Communications* 12.  
713 <https://doi.org/10.1038/s41467-021-21469-w>, 2021.
- 714 Gregoire, L. J., Ivanovic, R. F., Maycock, A. C., Valdes, P. J. & Stevenson, S.: Holocene lowering of the Laurentide ice  
715 sheet affects North Atlantic gyre circulation and climate. *Climate Dynamics* 51, 3797-3813.  
716 <https://doi.org/10.1007/s00382-018-4111-9>, 2018.
- 717 Gregoire, L. J., Payne, A. J. & Valdes, P. J.: Deglacial rapid sea level rises caused by ice-sheet saddle collapses. *Nature* 487,  
718 219-U1506. <https://doi.org/10.1038/nature11257>, 2012.
- 719 Gregoire, L. J., Valdes, P. J., Payne, A. J. & Kahana, R.: Optimal tuning of a GCM using modern and glacial constraints.  
720 *Climate Dynamics* 37, 705-719. <https://doi.org/10.1007/s00382-010-0934-8>, 2011.
- 721 Gregory, J. M., Browne, O. J. H., Payne, A. J., Ridley, J. K. & Rutt, I. C.: Modelling large-scale ice-sheet-climate  
722 interactions following glacial inception. *Climate of the Past* 8, 1565-1580. <https://doi.org/10.5194/cp-8-1565-2012>,  
723 2012.
- 724 Gregory, J. M., George, S. E. & Smith, R. S.: Large and irreversible future decline of the Greenland ice sheet. *Cryosphere*  
725 14, 4299-4322. <https://doi.org/10.5194/tc-14-4299-2020>, 2020.



- 726 Holden, P.B., Edwards, N.R., Oliver, K.I.C. *et al.*: A probabilistic calibration of climate sensitivity and terrestrial carbon  
727 change in GENIE-1. *Clim Dyn* 35, 785–806. <https://doi.org/10.1007/s00382-009-0630-8>, 2010.
- 728 Hughes, A. L. C., Gyllencreutz, R., Lohne, Ø. S., Mangerud, J., Svendsen, J. I.: The last Eurasian ice sheets – a  
729 chronological database and time-slice reconstruction, DATED-1. *Boreas*, Vol 45, pp. 1– 45. [10.1111/bor.12142](https://doi.org/10.1111/bor.12142). ISSN  
730 0300-9483, 2016.
- 731 Ivanovic, R. F. *et al.*: Acceleration of Northern Ice Sheet Melt Induces AMOC Slowdown and Northern Cooling in  
732 Simulations of the Early Last Deglaciation. *Paleoceanography and Paleoclimatology* 33, 807-824.  
733 <https://doi.org/10.1029/2017pa003308>, 2018.
- 734 Ivanovic, R. F. *et al.*: Transient climate simulations of the deglaciation 21-9 thousand years before present (version 1)-  
735 PMIP4 Core experiment design and boundary conditions. *Geoscientific Model Development* 9, 2563-2587.  
736 <https://doi.org/10.5194/gmd-9-2563-2016>, 2016.
- 737 Izumi, K., Valdes, P., Ivanovic, R. *et al.* Impacts of the PMIP4 ice sheets on Northern Hemisphere climate during the last  
738 glacial period. *Clim Dyn* 60, 2481–2499. <https://doi.org/10.1007/s00382-022-06456-1>, 2023.
- 739 Joshi, M. M., Webb, M. J., Maycock, A. C., and Collins, M.: Stratospheric water vapour and high climate sensitivity in a  
740 version of the HadSM3 climate model, *Atmos. Chem. Phys.*, 10, 7161–7167, <https://doi.org/10.5194/acp-10-7161-2010>,  
741 2010.
- 742 Lecavalier, B. S., Milne, G. A., Simpson, M. J. R., Wake, L., Huybrechts, P., Tarasov, L., Kjeldsen, K. K., Funder, S., Long,  
743 A. J., Woodroffe, S., Dyke, A. S., and Larsen, N. K.: A model of Greenland ice sheet deglaciation constrained by  
744 observations of relative sea level and ice extent, *Quaternary Sci. Rev.*, 102, 54–84,  
745 <https://doi.org/10.1016/j.quascirev.2014.07.018>, 2014.
- 746 Lee, V., Cornford, S., & Payne, A.: Initialization of an ice-sheet model for present-day Greenland. *Annals of Glaciology*,  
747 56(70), 129-140. doi:10.3189/2015AoG70A121, 2015.
- 748 Matero, I. S. O., Gregoire, L. J., and Ivanovic, R. F.: Simulating the Early Holocene demise of the Laurentide Ice Sheet with  
749 BISICLES (public trunk revision 3298), *Geosci. Model Dev.*, 13, 4555–4577, [https://doi.org/10.5194/gmd-13-4555-](https://doi.org/10.5194/gmd-13-4555-2020)  
750 2020, 2020.
- 751 Niu, L., Lohmann, G., Hinck, S., Gowan, E. J. & Krebs-Kanzow, U.: The sensitivity of Northern Hemisphere ice sheets to  
752 atmospheric forcing during the last glacial cycle using PMIP3 models. *Journal of Glaciology* 65, 645-661.  
753 <https://doi.org/10.1017/jog.2019.42>, 2019.
- 754 Obase, T., A. Abe-Ouchi, K. Kusahara, H. Hasumi, and R. Ohgaito, 2017: Responses of Basal Melting of Antarctic Ice  
755 Shelves to the Climatic Forcing of the Last Glacial Maximum and CO2 Doubling. *J. Climate*, **30**, 3473–3497,  
756 <https://doi.org/10.1175/JCLI-D-15-0908.1>.
- 757 Ogura, T., Abe-Ouchi, A., and Hasumi, H. (2004), Effects of sea ice dynamics on the Antarctic sea ice distribution in a  
758 coupled ocean atmosphere model, *J. Geophys. Res.*, 109, C04025, doi:10.1029/2003JC002022.
- 759 O’ishi, R. and Abe-Ouchi, A.: Influence of dynamic vegetation on climate change and terrestrial carbon storage in the Last  
760 Glacial Maximum, *Clim. Past*, 9, 1571–1587 (2013). <https://doi.org/10.5194/cp-9-1571-2013>
- 761 Kachuck, S. B., Martin, D. F., Bassis, J. N., & Price, S. F. (2020). Rapid viscoelastic deformation slows marine ice sheet  
762 instability at Pine Island Glacier. *Geophysical Research Letters*, 47, e2019GL086446.  
763 <https://doi.org/10.1029/2019GL086446>
- 764 Kageyama, M. *et al.* The PMIP4 Last Glacial Maximum experiments: preliminary results and comparison with the PMIP3  
765 simulations. *Climate of the Past* 17, 1065-1089 (2021). <https://doi.org/10.5194/cp-17-1065-2021>
- 766 Kageyama, M. *et al.* The PMIP4 contribution to CMIP6-Part 4: Scientific objectives and experimental design of the PMIP4-  
767 CMIP6 Last Glacial Maximum experiments and PMIP4 sensitivity experiments. *Geoscientific Model Development* 10,  
768 4035-4055 (2017). <https://doi.org/10.5194/gmd-10-4035-2017>



- 769 Klockmann, M., Mikolajewicz, U. & Marotzke, J. The effect of greenhouse gas concentrations and ice sheets on the glacial  
770 AMOC in a coupled climate model. *Climate of the Past* 12, 1829-1846 (2016). <https://doi.org/10.5194/cp-12-1829-2016>
- 771 Lofverstrom, M., Liakka, J. & Kleman, J. The North American Cordillera-An Impediment to Growing the Continent-Wide  
772 Laurentide Ice Sheet. *Journal of Climate* 28, 9433-9450 (2015). <https://doi.org/10.1175/jcli-d-15-0044.1>
- 773 Manabe, S. & Broccoli, A. J. THE INFLUENCE OF CONTINENTAL ICE SHEETS ON THE CLIMATE OF AN ICE-  
774 AGE. *Journal of Geophysical Research-Atmospheres* 90, 2167-2190 (1985). <https://doi.org/10.1029/JD090iD01p02167>
- 775 Martin Margold, Chris R. Stokes, Chris D. Clark, Reconciling records of ice streaming and ice margin retreat to produce a  
776 palaeogeographic reconstruction of the deglaciation of the Laurentide Ice Sheet, *Quaternary Science Reviews*, Volume  
777 189, 2018, Pages 1-30, ISSN 0277-3791, <https://doi.org/10.1016/j.quascirev.2018.03.013>.
- 778 Martin, D. F., Cornford, S. L., & Payne, A. J. (2019). Millennial-scale vulnerability of the Antarctic Ice Sheet to regional ice  
779 shelf collapse. *Geophysical Research Letters*, 46, 1467– 1475. <https://doi.org/10.1029/2018GL081229>
- 780 Murphy, J., Sexton, D., Barnett, D. *et al.* Quantification of modelling uncertainties in a large ensemble of climate change  
781 simulations. *Nature* 430, 768–772 (2004). <https://doi.org/10.1038/nature02771>
- 782 NOAA National Centers for Environmental Information (2023). State of the Climate: Global Climate Report for 2022.  
783 Accessed January 18, 2023, from <https://www.ncei.noaa.gov/access/monitoring/monthly-report/global/202213>.
- 784 Paul, A., Multiza, S., Stein, R. & Werner, M. A global climatology of the ocean surface during the Last Glacial Maximum  
785 mapped on a regular grid (GLOMAP). *Climate of the Past* 17, 805-824 (2021). <https://doi.org/10.5194/cp-17-805-2021>
- 786 Pico, T., Creveling, J. R. & Mitrovica, J. X. Sea-level records from the US mid-Atlantic constrain Laurentide Ice Sheet  
787 extent during Marine Isotope Stage 3. *Nature Communications* 8 (2017). <https://doi.org/10.1038/ncomms15612>
- 788 Pukelsheim, F. The Three Sigma Rule, *The American Statistician*, 48, 88–91, (1994). <https://doi.org/10.2307/2684253>
- 789 Quiquet, A., Roche, D. M., Dumas, C., Bouttes, N., and Lhardy, F.: Climate and ice sheet evolutions from the last glacial  
790 maximum to the pre-industrial period with an ice-sheet–climate coupled model, *Clim. Past*, 17, 2179–2199,  
791 <https://doi.org/10.5194/cp-17-2179-2021>, 2021.
- 792 Roche, D. M., Dumas, C., Bügelmayer, M., Charbit, S., and Ritz, C.: Adding a dynamical cryosphere to iLOVECLIM  
793 (version 1.0): coupling with the GRISLI ice-sheet model, *Geosci. Model Dev.*, 7, 1377–1394,  
794 <https://doi.org/10.5194/gmd-7-1377-2014>, 2014.
- 795 Roe, G. H. & Lindzen, R. S. The mutual interaction between continental-scale ice sheets and atmospheric stationary waves.  
796 *Journal of Climate* 14, 1450-1465 (2001). [https://doi.org/10.1175/1520-0442\(2001\)014<1450:tmibcs>2.0.co;2](https://doi.org/10.1175/1520-0442(2001)014<1450:tmibcs>2.0.co;2)
- 797 Rougier, J., D. M. H. Sexton, J. M. Murphy, and D. Stainforth, 2009: Analyzing the Climate Sensitivity of the HadSM3  
798 Climate Model Using Ensembles from Different but Related Experiments. *J. Climate*, 22, 3540–3557,  
799 <https://doi.org/10.1175/2008JCLI2533.1>.
- 800 Sanderson, B. M., 2011: A Multimodel Study of Parametric Uncertainty in Predictions of Climate Response to Rising  
801 Greenhouse Gas Concentrations. *J. Climate*, 24, 1362–1377, <https://doi.org/10.1175/2010JCLI3498.1>.
- 802 Schmittner, A., et al , Climate Sensitivity Estimated from Temperature Reconstructions of the Last Glacial Maximum.  
803 *Science* 334, 1385-1388(2011).DOI:10.1126/science.1203513
- 804 Sherriff-Tadano, S., Abe-Ouchi, A. & Oka, A.: Impact of mid-glacial ice sheets on deep ocean circulation and global  
805 climate. *Climate of the Past* 17, 95-110. <https://doi.org/10.5194/cp-17-95-2021>, 2021.
- 806 Sherriff-Tadano, S., Abe-Ouchi, A., Yoshimori, M., Hotta, H., Kikuchi, M., Ohgaito, R., Kodama, T., Vadsaria, T., Oka, A.,  
807 Suzuki, K.: Southern Ocean surface temperatures and cloud biases in climate models connected to the representation of  
808 glacial deep ocean circulation, *Journal of Climate*, (2023).
- 809 Shiogama, H., Watanabe, M., Yoshimori, M. *et al.*: Perturbed physics ensemble using the MIROC5 coupled atmosphere–  
810 ocean GCM without flux corrections: experimental design and results. *Clim Dyn* 39, 3041–3056.  
811 <https://doi.org/10.1007/s00382-012-1441-x>, 2012.





- 812 Smith, R. S.: The FAMOUS climate model (versions XFXWB and XFHCC): description update to version XDBUA.  
813 Geoscientific Model Development 5, 269-276. <https://doi.org/10.5194/gmd-5-269-2012>, 2012.
- 814 Smith, R. S., George, S. & Gregory, J. M. FAMOUS version xotzt (FAMOUS-ice): a general circulation model (GCM)  
815 capable of energy- and water-conserving coupling to an ice sheet model. Geoscientific Model Development 14, 5769-  
816 5787. <https://doi.org/10.5194/gmd-14-5769-2021>, 2021.
- 817 Smith, R. S., Mathiot, P., Siahhan, A., Lee, V., Cornford, S. L., Gregory, J. M., et al.: Coupling the U.K. Earth System model  
818 to dynamic models of the Greenland and Antarctic ice sheets. *Journal of Advances in Modeling Earth Systems*, 13,  
819 e2021MS002520. <https://doi.org/10.1029/2021MS002520>, 2021.
- 820 Smith, R. S. & Gregory, J.: The last glacial cycle: transient simulations with an AOGCM. *Climate Dynamics* 38, 1545-1559.  
821 <https://doi.org/10.1007/s00382-011-1283-y>, 2012.
- 822 Smith, R. S., Gregory, J. M. & Osprey, A.: A description of the FAMOUS (version XDBUA) climate model and control run.  
823 Geoscientific Model Development 1, 53-68. <https://doi.org/10.5194/gmd-1-53-2008>, 2008.
- 824 Smith, R.N.B.: A scheme for predicting layer clouds and their water content in a general circulation model. *Q.J.R. Meteorol.*  
825 *Soc.*, 116: 435-460. <https://doi.org/10.1002/qj.49711649210>, 1990.
- 826 Tabone, I., Blasco, J., Robinson, A., Alvarez-Solas, J., and Montoya, M.: The sensitivity of the Greenland Ice Sheet to  
827 glacial-interglacial oceanic forcing. *Clim. Past*, 14, 455-472, <https://doi.org/10.5194/cp-14-455-2018>, 2018.
- 828 Tarasov, L., Dyke, A. S., Neal, R. M. & Peltier, W. R.: A data-calibrated distribution of deglacial chronologies for the North  
829 American ice complex from glaciological modeling. *Earth and Planetary Science Letters* 315, 30-40.  
830 <https://doi.org/10.1016/j.epsl.2011.09.010>, 2012.
- 831 Tierney, J. E. et al.: Glacial cooling and climate sensitivity revisited. *Nature* 584, 569+. [https://doi.org/10.1038/s41586-020-](https://doi.org/10.1038/s41586-020-2617-x)  
832 [2617-x](https://doi.org/10.1038/s41586-020-2617-x), 2020.
- 833 Tsai, V., Stewart, A., & Thompson, A.: Marine ice-sheet profiles and stability under Coulomb basal conditions. *Journal of*  
834 *Glaciology*, 61(226), 205-215. doi:10.3189/2015JoG14J221, 2015.
- 835 van de Wal, R. S. W., Boot, W., Smeets, C. J. P. P., Snellen, H., van den Broeke, M. R., and Oerlemans, J.: Twenty-one  
836 years of mass balance observations along the K-transect, West Greenland, *Earth Syst. Sci. Data*, 4, 31-35,  
837 <https://doi.org/10.5194/essd-4-31-2012>, 2012.
- 838 Van Liefferinge, B., Taylor, D., Tsutaki, S., Fujita, S., Gogineni, P., Kawamura, K., et al.: Surface mass balance controlled  
839 by local surface slope in inland Antarctica: Implications for ice-sheet mass balance and Oldest Ice delineation in Dome  
840 Fuji. *Geophysical Research Letters*, 48, e2021GL094966. <https://doi.org/10.1029/2021GL094966>, 2021.
- 841 Vizcaino, M. et al.: Greenland Surface Mass Balance as Simulated by the Community Earth System Model. Part I: Model  
842 Evaluation and 1850-2005 Results. *Journal of Climate* 26, 7793-7812. <https://doi.org/10.1175/jcli-d-12-00615.1>, 2013.
- 843 Williamson, D. Exploratory ensemble designs for environmental models using k-extended latin hypercubes. *Environmetrics*,  
844 26 (4), 268-283 (2015). <https://onlinelibrary.wiley.com/doi/full/10.1002/env.2335>
- 845 Williams, K. D., Senior, C. A. and Mitchell, J. F. B.: Transient Climate Change in the Hadley Centre Models: The Role of  
846 Physical Processes. *J. Climate*, 14, 2659-2674, [https://doi.org/10.1175/1520-0442\(2001\)014<2659:TCCITH>2.0.CO;2](https://doi.org/10.1175/1520-0442(2001)014<2659:TCCITH>2.0.CO;2),  
847 2001.
- 848 Willeit, M. & Ganopolski, A.: The importance of snow albedo for ice sheet evolution over the last glacial cycle. *Climate of*  
849 *the Past* 14, 697-707. <https://doi.org/10.5194/cp-14-697-2018>, 2018.
- 850 Yamagishi, T., Abe-Ouchi, A., Saito, F., Segawa, T., & Nishimura, T.: Re-evaluation of paleo-accumulation  
851 parameterization over Northern Hemisphere ice sheets during the ice age examined with a high-resolution AGCM and a  
852 3-D ice-sheet model. *Annals of Glaciology*, 42, 433-440. doi:10.3189/172756405781813032, 2005.
- 853 Ziemen, F. A., Rodehacke, C. B., and Mikolajewicz, U.: Coupled ice sheet-climate modeling under glacial and pre-industrial  
854 boundary conditions, *Clim. Past*, 10, 1817-1836, <https://doi.org/10.5194/cp-10-1817-2014>, 2014.





855    Zhu, J., Otto-Bliesner, B., Brady, E., Poulsen, C.J., Shaw, J.K., Kay, J.E. LGM paleoclimate constraints inform cloud  
856        parameterizations and equilibrium climate sensitivity in CESM2. *Journal of Advances in Modeling Earth Systems*, 14(4),  
857        e2021MS002776. <https://doi.org/10.1029/2021MS002776>, 2022.  
858    Zhu, J. and Poulsen, C. J.: Last Glacial Maximum (LGM) climate forcing and ocean dynamical feedback and their  
859        implications for estimating climate sensitivity, *Clim. Past*, 17, 253–267, <https://doi.org/10.5194/cp-17-253-2021>, 2021.  
860